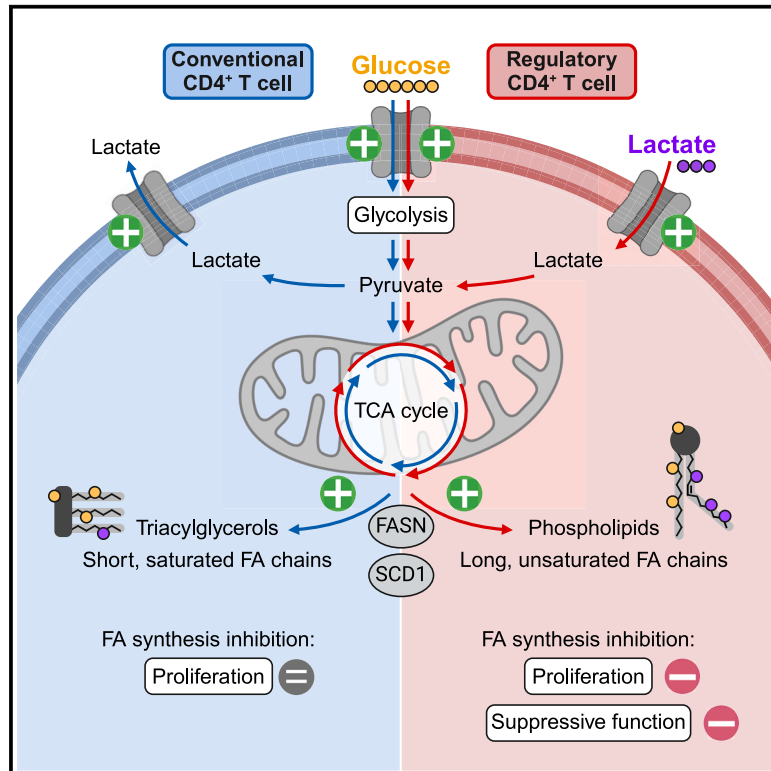


# Immune suppression by human thymus-derived effector Tregs relies on glucose/lactate-fueled fatty acid synthesis

## Graphical abstract



## Authors

Sander de Kivit, Mark Mensink, Sarantos Kostidis, ..., Celia R. Berkers, Martin Giera, Jannie Borst

## Correspondence

s.de\_kivit@lumc.nl (S.d.K.), j.g.borst@lumc.nl (J.B.)

## In brief

de Kivit et al. reveal discerning lipidomes of conventional T cells (Tconvs) versus thymus-derived regulatory T cells (tTreg). Effector tTregs can use either glucose or lactate to synthesize long and unsaturated fatty acids, on which they rely for proliferation and suppressive function. These tTreg-specific properties may be therapeutically exploited.

## Highlights

- Human conventional (Tconv) and regulatory T (Treg) cells have distinct lipidomes
- TNFR2-driven glycolysis links to fatty acid synthesis (FAS) in Tregs but not Tconvs
- Treg proliferation relies on FAS fueled by glucose or lactate
- Treg suppressive function relies on synthesis of unsaturated fatty acids



## Article

# Immune suppression by human thymus-derived effector Tregs relies on glucose/lactate-fueled fatty acid synthesis

Sander de Kivit,<sup>1,2,5,7,\*</sup> Mark Mensink,<sup>1,2,5</sup> Sarantos Kostidis,<sup>3</sup> Rico J.E. Derks,<sup>3</sup> Esther A. Zaal,<sup>4</sup> Marieke Heijink,<sup>3</sup> Lotte J. Verleng,<sup>1,2</sup> Evert de Vries,<sup>1,2</sup> Ellen Schrama,<sup>1,2</sup> Niek Blomberg,<sup>3</sup> Celia R. Berkers,<sup>4</sup> Martin Giera,<sup>3,6</sup> and Jannie Borst<sup>1,2,6,\*</sup>

<sup>1</sup>Department of Immunology, Leiden University Medical Center, 2300 RC Leiden, the Netherlands

<sup>2</sup>OncoCode Institute, Leiden University Medical Center, 2300 RC Leiden, the Netherlands

<sup>3</sup>Center for Proteomics and Metabolomics, Leiden University Medical Center, 2300 RC Leiden, the Netherlands

<sup>4</sup>Division of Cell Biology, Metabolism, and Cancer, Department of Biomolecular Health Sciences, Faculty of Veterinary Medicine, Utrecht University, 3584 CM Utrecht, the Netherlands

<sup>5</sup>These authors contributed equally

<sup>6</sup>Senior author

<sup>7</sup>Lead contact

\*Correspondence: [s.de\\_kivit@lumc.nl](mailto:s.de_kivit@lumc.nl) (S.d.K.), [j.g.borst@lumc.nl](mailto:j.g.borst@lumc.nl) (J.B.)

<https://doi.org/10.1016/j.celrep.2024.114681>

## SUMMARY

Regulatory T cells (Tregs) suppress pro-inflammatory conventional T cell (Tconv) responses. As lipids impact cell signaling and function, we compare the lipid composition of CD4<sup>+</sup> thymus-derived (t)Tregs and Tconvs. Lipidomics reveal constitutive enrichment of neutral lipids in Tconvs and phospholipids in tTregs. TNFR2-co-stimulated effector tTregs and Tconvs are both glycolytic, but only in tTregs are glycolysis and the tricarboxylic acid (TCA) cycle linked to a boost in fatty acid (FA) synthesis (FAS), supported by relevant gene expression. FA chains in tTregs are longer and more unsaturated than in Tconvs. In contrast to Tconvs, tTregs effectively use either lactate or glucose for FAS and rely on this process for proliferation. FASN and SCD1, enzymes responsible for FAS and FA desaturation, prove essential for the ability of tTregs to suppress Tconvs. These data illuminate how effector tTregs can thrive in inflamed or cancerous tissues with limiting glucose but abundant lactate levels.

## INTRODUCTION

The cluster of differentiation 4-positive (CD4<sup>+</sup>) T cell lineage encompasses conventional T cells (Tconvs) and regulatory T cells (Tregs) that are functional opposites. While Tconvs orchestrate and mediate immune responses against pathogens, Tregs suppress self-reactive and excessive Tconv responses to prevent autoimmunity.<sup>1</sup> Tregs use a variety of suppressive mechanisms, including CTLA4-mediated downregulation of co-stimulatory ligands CD80 and CD86 from dendritic cells and hydrolysis of pro-inflammatory ATP into immunosuppressive adenosine.<sup>1</sup> Tregs also control tissue homeostasis by preventing inflammatory immune responses to dying cells and making specific factors that promote tissue repair.<sup>2,3</sup> Adoptive cell therapy with Tregs is therefore a promising approach in autoimmune and inflammatory diseases and in transplant rejection.<sup>4</sup> In cancer and chronic infections, Tregs hamper desired Tconv activity, and Treg inhibition or depletion is an important therapeutic approach.<sup>5,6</sup>

Thymus-derived (t)Tregs develop as a stable CD4<sup>+</sup> T cell lineage within the thymus. They are positively selected on recognition of self-antigens and control both systemic and tissue-specific autoimmunity.<sup>7,8</sup> Treg identity is predominantly controlled

by the transcription factor FOXP3, which orchestrates tTreg development and function.<sup>9–12</sup> When responding to non-self-antigens, CD4<sup>+</sup> Tconvs may also acquire FOXP3 expression and therewith Treg functions. These peripherally induced (p)Tregs are primarily found in the digestive tract.<sup>13</sup> Like Tconvs, tTregs circulate in their naive state through blood and secondary lymphoid tissues, but they can also clonally expand and differentiate into effector cells that migrate to and become resident in non-lymphoid tissues (NLTs).<sup>14</sup> Different from Tconvs, tTregs do not express the interleukin-7 (IL-7) receptor (CD127) and constitutively express the IL-2 receptor (CD25). They rely on IL-2 for their survival and clonal expansion, which is primarily supplied by Tconvs.<sup>1</sup> Both healthy and diseased NLTs harbor tTregs that in response to cytokines secreted by Tconvs and other environmental factors can gain expression of transcription factors T-bet, ROR $\gamma$ T, or GATA3.<sup>14,15</sup> In Tconvs, these factors dictate T helper subset differentiation, but in effector tTregs, they differentially regulate gene expression and function without compromising suppressive functions.<sup>14</sup>

Core transcriptomic<sup>16–19</sup> and proteomic<sup>20,21</sup> signatures discriminate tTregs from Tconvs, regardless of their activation state. In both Tconvs and tTregs, signaling via the T cell antigen



receptor (TCR)<sup>22</sup> and co-stimulatory and cytokine receptors<sup>23</sup> regulates cell survival, clonal expansion, and effector differentiation. Compared to Tconvs, tTregs rely and respond differentially to the same receptors in terms of gene expression and function. For instance, tTregs cannot make IL-2 upon their activation via the TCR, even in the presence of CD28 co-stimulation.<sup>13,24,25</sup> One explanation for differential wiring of signal transduction pathways downstream of cell surface receptors is the pairing of FOXP3 with certain transcription factors and the concomitant alteration in gene targeting specificity of the heterodimers.<sup>20,26,27</sup> Furthermore, tTregs and Tconvs display constitutive differences in the expression of certain signal transduction components, such as signal transducer and activator of transcription and nuclear factor  $\kappa$ B (NF- $\kappa$ B) family members, which prevents them from being pro-inflammatory.<sup>20</sup> It is becoming apparent that T cell numbers, fate, and functionality are not only dictated by TCR, co-stimulatory, and cytokine input but also by nutrient availability and associated metabolic adaptations.<sup>28</sup> Since the balance between tTreg and Tconv numbers and their functionality dictates the outcome of immune responses, it is essential to understand the impact of all these stimuli and processes in Tregs and Tconvs.<sup>28</sup>

We have recently investigated using multi-omics the differential impact of co-stimulatory receptors CD28 and tumor necrosis factor receptor 2 (TNFR2) on human CD4<sup>+</sup> tTregs and Tconvs. TNFR2 proved to be an important co-stimulus for tTregs that induces them to adopt a gene expression profile as found in NLT-resident tTregs in health and disease, characterized by shape changes, improved cell motility, and suppressive activity.<sup>29</sup> In contrast, after CD28 co-stimulation, tTregs maintain a lymphoid tissue-resident (central Treg) phenotype. Only after TNFR2 co-stimulation did tTregs become glycolytic, whereas Tconvs did so regardless of the costimulus.<sup>30</sup> Here, we analyzed the lipid composition of human CD4<sup>+</sup> Tconvs and tTregs at steady state and under different co-stimulatory conditions. We rationalized that lipids may govern cell identity, differentiation, and function as structural membrane components<sup>31</sup> and by their impact on cell signaling (e.g., as components of lipid rafts,<sup>32–34</sup> as docking sites for signaling molecules,<sup>35</sup> or as signaling molecules themselves<sup>36,37</sup>). Lipid biosynthesis is intimately linked to cell metabolism<sup>38</sup>; therefore, it can be envisioned how the cellular environment can impact the tTreg/Tconv balance in healthy and diseased tissues, by dictating the availability of TCR, co-stimulatory, and cytokine signals, as well as nutrients. Our study shows inherent differences in lipid composition between tTregs and Tconvs and a discerning glucose/lactate-fueled pathway for *de novo* fatty acid (FA) synthesis (FAS) in TNFR2-co-stimulated effector tTregs, which they rely on for their proliferation and suppressive function.

## RESULTS

### The lipidomes of human tTregs and Tconvs are distinct and remodeled upon TNFR2 co-stimulation

Naive tTregs and Tconvs from healthy donor blood were flow cytometrically sorted as described<sup>29,30,39</sup> (Figure S1A), expanded by stimulation with agonistic monoclonal antibodies (mAbs) against the TCR/CD3 complex and CD28 in the presence of

IL-2, and subsequently made quiescent (Figure S1B). The obtained tTreg population was uniformly positive for FOXP3, Helios (IKZF2), and CTLA4, and expressed TNFR2 (Figure S1C). The resulting tTregs and Tconvs were stimulated for 24 h by CD3 engagement with either CD28 or TNFR2 co-stimulation, or they were left unstimulated (Figure S1B), followed by examination of their lipid composition by untargeted lipidomics. Principal-component analysis (PCA) of the lipidomes segregated tTregs from Tconvs in PC1, revealing cell-type-specific differences, while PC2 identified that tTregs and Tconvs altered their lipidome in response to CD3/28 or CD3/TNFR2 stimulation (Figure 1A). Especially in tTregs, CD3/TNFR2 stimulation altered the lipid composition more dramatically than did CD3/28 stimulation (Figure 1A).

Examination of the lipid classes revealed a higher abundance in tTregs of phospholipids (phosphatidic acid [PA], phosphatidylcholine [PC], phosphatidylethanolamine [PE], phosphatidylglycerol [PG], phosphatidylinositol [PI], phosphatidylserine [PS]) and a higher abundance of (ether)di- and triacylglycerols ((O)-DG, (O)-TG) and ether-phospholipids (O-PC, O-PE, O-PI, O-LPC [lysophosphatidylcholine]) in Tconvs (Figure 1B). In line with PCA (Figure 1A), the cell stimuli did not affect this difference in lipid composition between tTregs and Tconvs (Figure 1B). Examination of the lipid classes before and after stimulation indicated that in Tconvs, either CD3/28 or CD3/TNFR2 stimulation primarily increased DG/TG content (Figure 1C). In tTregs, only CD3/TNFR2 stimulation triggered a lipidomic response and also primarily increased DG/TG content (Figure 1D). TNFR2 co-stimulation specifically induced in both cell types an increase in phospholipid levels (Figures 1C and 1D). These observations were confirmed by a targeted, quantitative analysis using the Lipidizer platform<sup>40,41</sup> (Figure S2). Collectively, these data indicate that human tTregs and Tconvs can be distinguished based on overall lipid composition and that Tconvs remodel their lipidome upon activation, regardless of the co-stimulus. For activated tTregs, however, TNFR2 co-stimulation proves to be a driver of lipidome remodeling.

### tTregs have lipids with long, unsaturated FAs that increase in abundance upon TNFR2 co-stimulation

To further define the lipidomes of tTregs and Tconvs, we examined the FA side chain moieties in phospholipids and glycerolipids, since their abundance greatly differed between the cell types. Hierarchical clustering based on FA moieties (Figures 2A and S3A) revealed PC, PE, and PG species in clusters 2, 6, and 8 that were mainly present in tTregs, while the same phospholipid species in clusters 1, 4, and 7 were mainly present in Tconvs (Figures 2A and S4A–S4C). In addition, we identified PC, PE, and PG species in clusters 3, 5, 6, and 8 that were selectively increased in tTregs upon TNFR2 co-stimulation (Figures 2A and S4A–S4C). Other phospholipid species trended to be upregulated in both Tconvs and tTregs after TNFR2 co-stimulation (Figure S3A). Regarding TG (Figures 2B and S3B), tTregs and Tconvs specifically increased content upon CD3/TNFR2 stimulation, in line with previous findings (Figures 1C and 1D). Hierarchical clustering based on the FA moieties revealed that the upregulated TGs were partially unique in composition for either Tconvs (cluster 1) or tTregs (cluster 4), while a smaller fraction

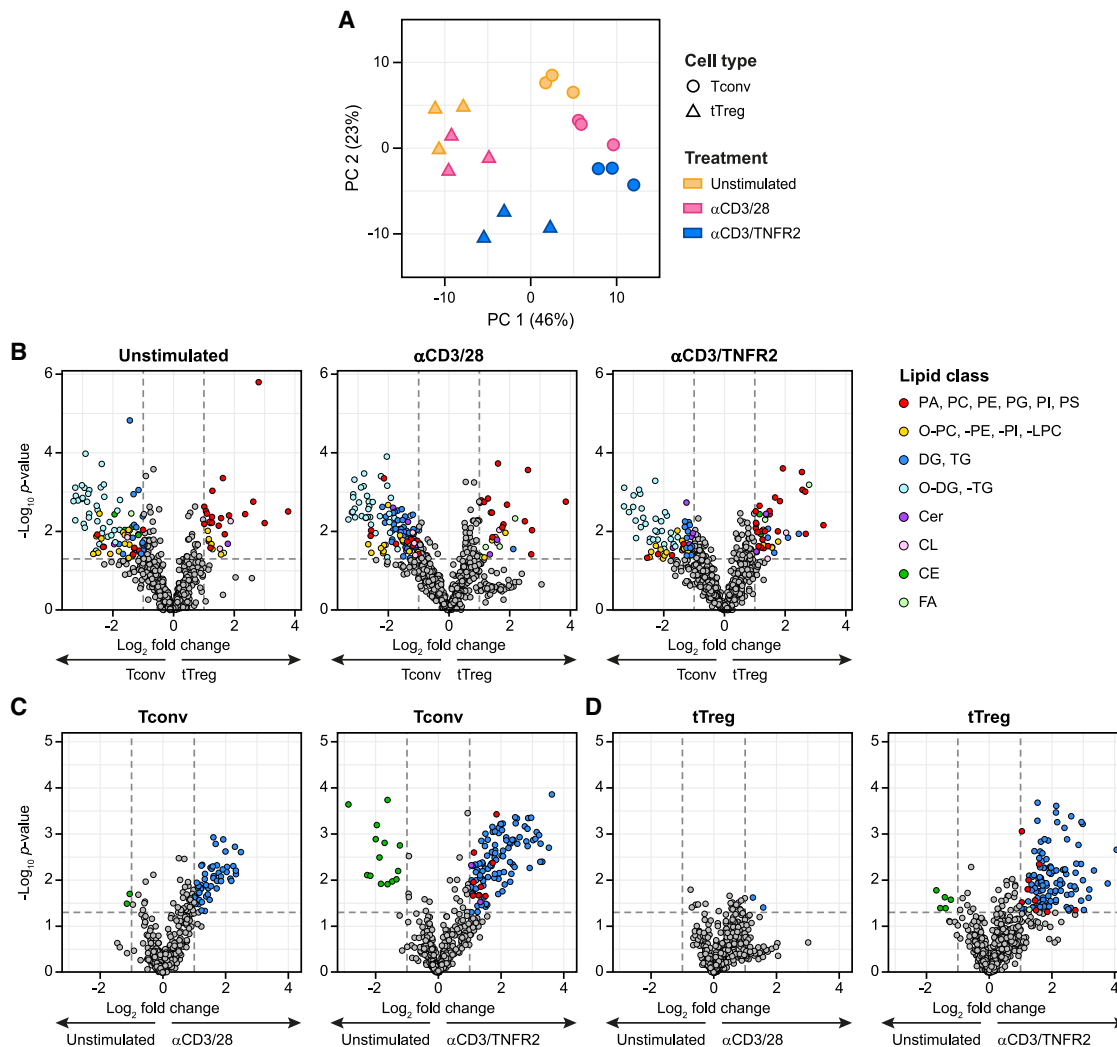


**Figure 1. The lipidomes of human tTregs and Tconvs are distinct and remodeled upon TNFR2 co-stimulation**

(A) PCA plot of untargeted lipidomic analysis of expanded tTregs and Tconvs that were activated as indicated. Unstimulated cells served as controls.

(B) Volcano plots comparing the abundance of indicated lipid classes between tTregs and Tconvs under the indicated stimulation conditions.

(C and D) Differences in lipid class abundance upon activation in Tconvs (C) or tTregs (D) under indicated stimulation conditions.

(B–D) Each dot represents one lipid, and lipid classes are color-coded when  $p < 0.05$  and  $\log_2$  fold change  $> 1$  or  $< -1$ . Unpaired two-sided Student's *t* test was used for statistical analysis;  $p = 0.05$  is indicated by the dashed horizontal line. Data represent  $n = 3$  samples from individual donors in independent cultures CE, cholesteryl ester; Cer, ceramide; CL, cardiolipin; O-, ether.

See also Figures S1 and S2.

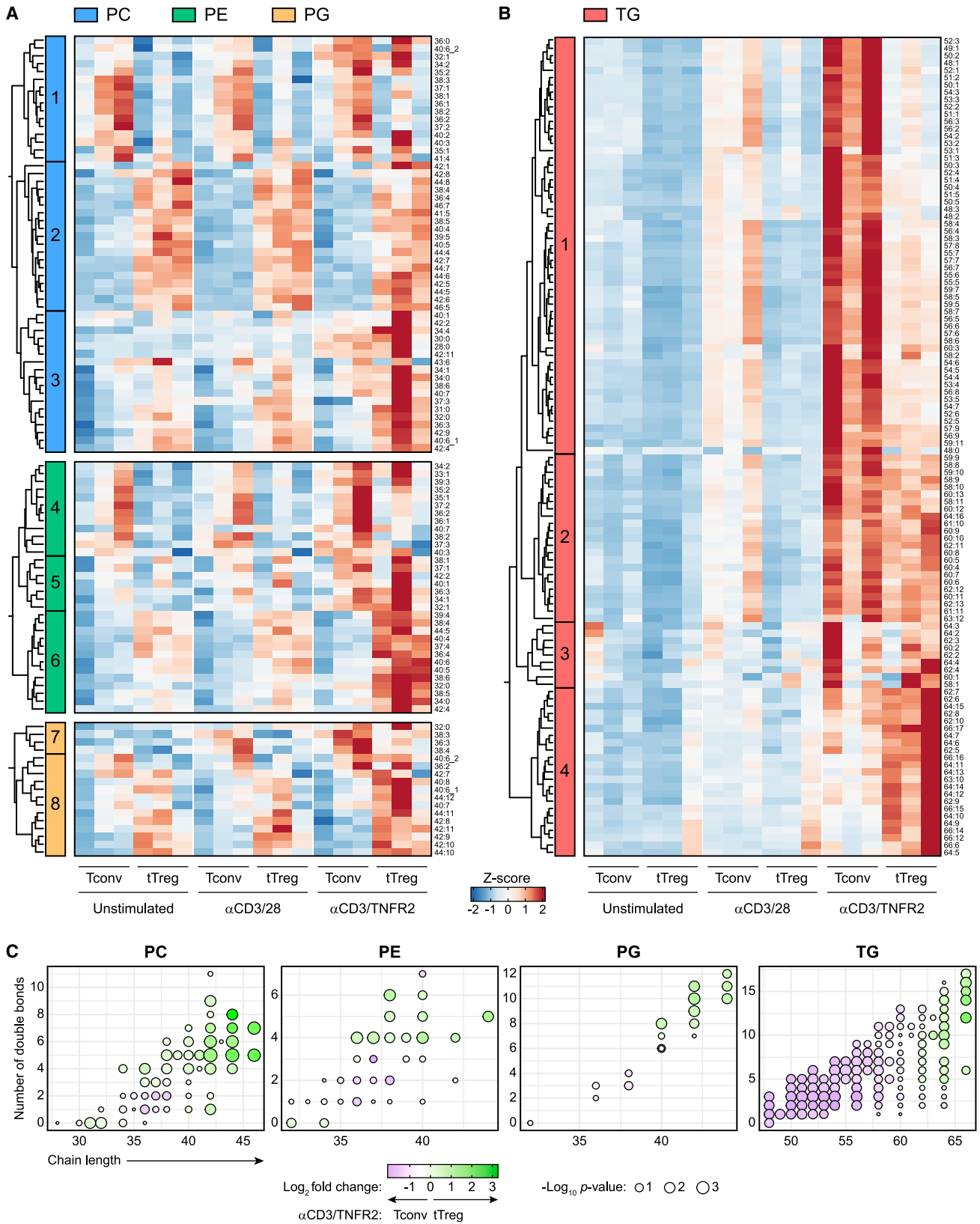
had the same composition in both cell types (cluster 2) (Figures 2B and S4D). The analysis also revealed that Tconvs were exclusively enriched for ether-TG (Figure S3B).

To shed light on the differential composition of the PC, PE, PG, and TG species in tTregs and Tconvs, we plotted the FA chain length against the number of double bonds within them. This analysis revealed that FA chains in all these lipid classes were longer and had more double bonds in tTregs as compared to Tconvs regardless of the co-stimulus provided to them (Figures 2C, S3C, and S3D). We conclude that tTregs and Tconvs have baseline differences in phospholipid composition, that both cell types respond to TNFR2 co-stimulation by increasing phospholipid and TG content, but that all these lipid

species contain longer and more unsaturated FAs in tTregs as compared to Tconvs.

### TNFR2 co-stimulation boosts lipid synthesis in tTregs at the transcriptional level

To understand how TNFR2 co-stimulation caused lipid composition remodeling, we performed unbiased transcriptome analysis in tTregs and Tconvs. PCA revealed distinct gene expression profiles in tTregs versus Tconvs in PC1, as expected from the different nature of the cell types (Figure 3A). PC2 revealed that tTregs responded more strongly to co-stimulation via TNFR2 as compared to CD28, while the transcriptome of activated Tconvs was not greatly affected by either co-stimulus (Figure 3A).



(legend on next page)

We have reported that TNFR2-, but not CD28 co-stimulation, induces a glycolytic switch in activated tTregs and differentially affects the metabolic state of tTregs and Tconvs.<sup>30,43</sup> To examine whether metabolic alterations in tTregs as induced by TNFR2 co-stimulation were linked to lipid biosynthesis, we performed gene set enrichment analysis (GSEA) using curated gene sets related to metabolism.<sup>42</sup> GSEA revealed that besides glycolysis, pathways involved in lipid and nucleotide metabolism were upregulated in TNFR2-co-stimulated tTregs. Lipid metabolism pathways included biosynthesis of cholesterol and unsaturated FA, and identified sterol regulatory element-binding proteins (SREBPs) as potential upstream regulators (Figures 3B and S5A). Ingenuity Pathway Analysis (IPA) indeed identified *SREBF1* and *SREBF2* among potential upstream regulators of the TNFR2-driven gene expression program in activated tTregs (Figure 3C). *SREBF1* is known to drive FAS, while *SREBF2* stimulates cholesterol synthesis.<sup>44</sup> *SREBF1* was specifically upregulated in TNFR2-co-stimulated tTregs, while *SREBF2* was upregulated in both TNFR2-co-stimulated tTregs and Tconvs (Figure 3D). STRING network analysis of SREBP target genes that were specifically affected by TNFR2 co-stimulation in activated tTregs revealed a cluster of genes encoding key enzymes involved in FAS (*ACACA*, *ACLY*, and *FASN*), FA desaturation (*FADS1* and *SCD*), and cholesterol biosynthesis (*HMGCS1*, *HMGCR*, *MVD*, *FDPS*, *FDFT1*, *SQLE*, and *DHCR7*) (Figure 3E). Comparative analysis of lipid metabolism-related transcripts in CD3-, CD3/28-, and CD3/TNFR2-stimulated cells showed that in tTregs TNFR2 co-stimulation specifically upregulated molecules involved in lipid biosynthesis (*GK*, *SLC25A1*, *ACLY*, *ACACA*, *FASN*, and *SCD*) and downregulated molecules involved in lipid breakdown through the  $\beta$ -oxidation pathway (*PNPLA2/ATGL*, *ACSS2*, *ACADS*, *ACSL6*, *CPT1A*, and *ACSF2*) (Figure 3F). In contrast, TNFR2 or CD28 co-stimulation did not affect the expression of any of these genes in Tconvs (Figure S5B), most likely because CD3 stimulation alone is already sufficient for metabolic rewiring in these cells.<sup>45</sup>

We have previously reported that TNFR2 co-stimulation enables differentiation of tTregs into effector cells with the core qualities of NLT-resident tTregs, while CD28 co-stimulation maintains an LT-resident, central tTreg phenotype.<sup>29</sup> To address whether an FAS-associated gene signature is also apparent in Tregs found *in vivo*, we compared the transcriptome of CD3/TNFR2-activated tTregs with that of tumor Tregs published by Lim et al.<sup>42</sup> GSEA showed that the genes upregulated in TNFR2-co-stimulated tTregs are enriched in these tumor Tregs (Figure 3G). Comparison of FAS-associated genes, as annotated in the Kyoto Encyclopedia of Genes and Genomes (KEGG) database, revealed that genes encoding enzymes involved in FA desaturation (*SCD*, *FADS1*, and *FADS2*), FA elongation (*ELOVL6*),

and TG biosynthesis (*DGAT2*) were upregulated in both CD3/TNFR2-activated tTregs and tumor Tregs (Figure 3H). The collective data suggest that TNFR2-co-stimulated tTregs display a program geared toward biosynthesis of unsaturated FA, which can also be found *in vivo*.

### Glucose fuels lipid biosynthesis in TNFR2-co-stimulated tTregs

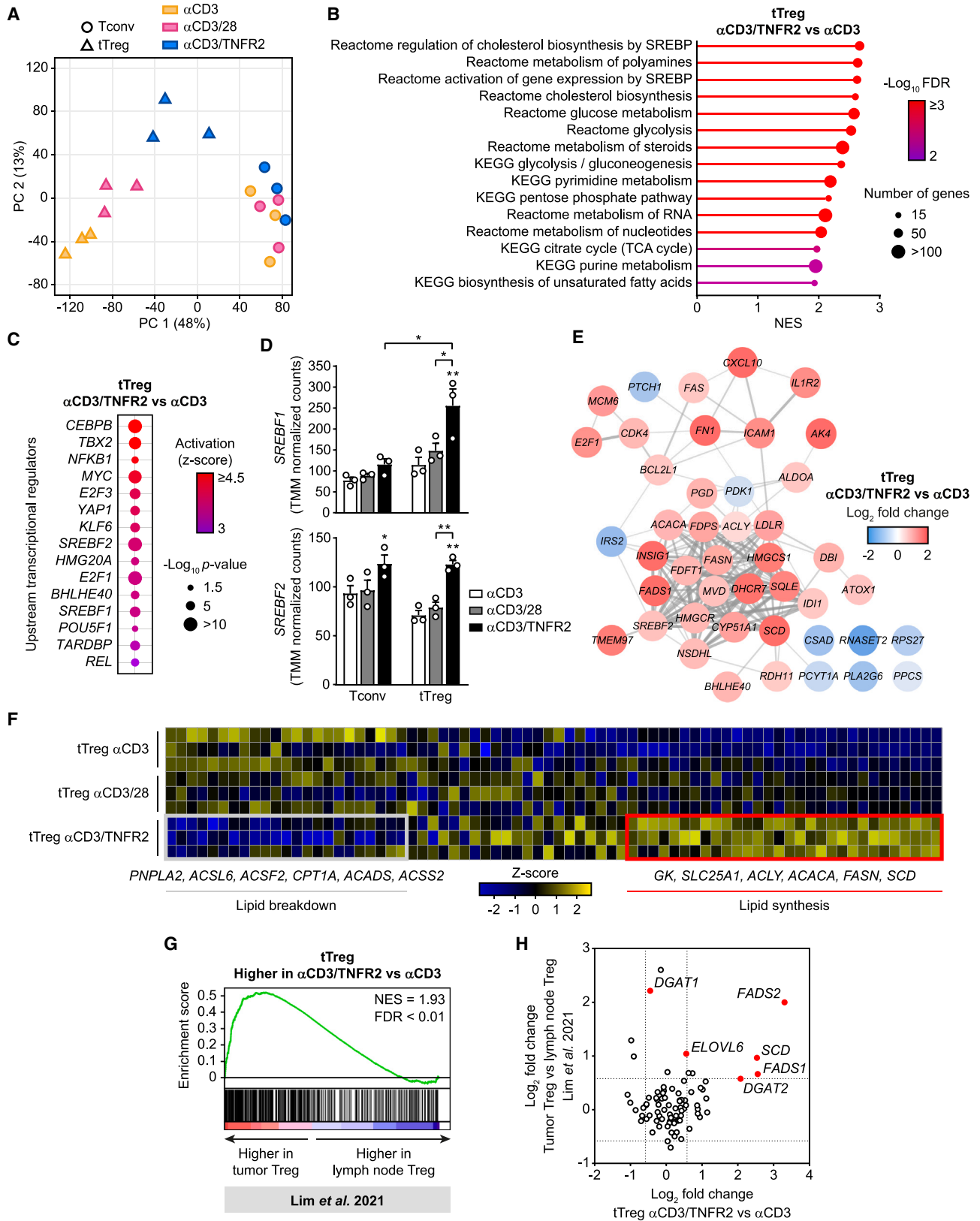
FA needed for lipid biosynthesis may be taken up by cells from their environment and/or synthesized *de novo*. To examine the FA uptake capacity of tTregs and Tconvs, we presented them with the fluorescent palmitate analog BODIPY-C<sub>12</sub>. While Tconvs readily increased FA uptake upon activation by either CD3/28 or CD3/TNFR2, tTregs showed a significantly lower FA uptake capacity under either condition (Figure 4A). This finding suggests that tTregs rely on other nutrient sources for lipid biosynthesis after TNFR2 co-stimulation. TNFR2 co-stimulation supports glycolysis in tTregs<sup>30</sup> and therefore glucose might be a required carbon source for lipid biosynthesis. Uptake of the fluorescent glucose analog 6-NBDG was increased in Tconvs after activation, regardless of the co-stimulus, while in tTregs only TNFR2 co-stimulation boosted glucose uptake to levels similar to those in Tconvs (Figure 4B). These data suggest glucose as a potential nutrient for lipid biosynthesis in TNFR2-co-stimulated tTregs.

Glucose-derived carbon can be used for *de novo* FAS via glycolysis and the associated tricarboxylic acid (TCA) cycle, from where mitochondrial citrate can be transported into the cytosol. The enzyme *ACLY* generates acetyl-coenzyme A (CoA) from citrate, which is used among others, for FAS (Figure 4C). To examine the fate of glucose-derived carbon, we fed tTregs and Tconvs with [U-<sup>13</sup>C<sub>6</sub>]-glucose under the different stimulation conditions and traced glucose-derived <sup>13</sup>C throughout the intermediates of glycolysis and the TCA cycle (Figure 4C). While Tconvs became glycolytic after activation regardless of the co-stimulus, tTregs did so only after TNFR2 co-stimulation, as indicated by the increased levels of <sup>13</sup>C-labeled pyruvate and lactate (Figures 4D and S6A). Intracellular levels of <sup>13</sup>C-labeled lactate were similar in tTregs and Tconvs upon CD3/TNFR2 stimulation (Figure 4D), but tTregs secreted lactate to a lesser extent (Figure S6B), as observed previously.<sup>30</sup> TNFR2-co-stimulated tTregs shuttled glucose-derived carbon into the TCA cycle, as demonstrated by increased <sup>13</sup>C-labeling of citrate (Figure 4E). While <sup>13</sup>C-labeled and total citrate levels were equal in glycolytic tTregs and Tconvs, levels of <sup>13</sup>C- $\alpha$ -ketoglutarate and <sup>13</sup>C-malate, as well as total levels of these metabolites, were reduced in tTregs as compared to Tconvs (Figures 4E and S6C). This suggests that in glycolytic tTregs, citrate exits the TCA cycle to act as a source for lipid biosynthesis.

### Figure 2. tTregs have lipids with long, unsaturated FAs that increase in abundance upon TNFR2 co-stimulation

(A and B) Heatmaps displaying hierarchical clustering based on FA moieties within phospholipid classes PC, PE, and PG (A) and TG (B) in tTregs and Tconvs stimulated as indicated. FA moieties within each lipid are annotated by their carbon chain length and degree of unsaturation (e.g., a lipid annotated as 34:2 contains FAs with combined chain length of 34 carbons, with 2 double bonds present). Z scores are color-coded. (C) Visualization of FA distribution based on their acyl chain length and number of double bonds within PC, PE, PG, and TG. Green: FA moieties enriched in CD3/TNFR2-stimulated tTregs; purple: FA moieties enriched in CD3/TNFR2-stimulated Tconvs. Data represent *n* = 3 samples from individual donors in independent cultures.

See also Figures S3 and S4.



(legend on next page)

To determine whether glycolytic tTregs indeed use glucose for lipid biosynthesis, we traced glucose-derived  $^{13}\text{C}$  into FA, PC, and TG. Activated tTregs and Tconvs both exhibited increased  $^{13}\text{C}$ -labeling into FA, as well as in the glycerol backbone of PC and TG, upon CD3-mediated activation and either CD28 or TNFR2 co-stimulation (Figure 4F). In tTregs, this was most pronounced after TNFR2 co-stimulation, and incorporation of  $^{13}\text{C}$  in PC was higher than in Tconvs under this condition, while incorporation of  $^{13}\text{C}$  in TG was lower in tTregs than in Tconvs after both CD28 and TNFR2 co-stimulation (Figure 4F). LipidTOX staining corroborated an increase in neutral lipid content in both tTregs and Tconvs after stimulation, while a higher level was observed in Tconvs as compared to tTregs (Figure S6D). In summary, these data indicate that glycolytic tTregs and Tconvs both use glucose for *de novo* FA, phospholipid, and TG synthesis, but glucose-derived carbons are primarily incorporated into phospholipids in tTregs and into TG in Tconvs.

### tTregs but not Tconvs use lactate for FAS upon glucose deprivation

We have found that TNFR2 co-stimulation in tTregs induces a gene expression signature characteristic for effector tTregs found in healthy and diseased NLTs.<sup>29</sup> This is illustrated by GSEA, which indicates enrichment of a human pan-cancer Treg gene expression signature<sup>46</sup> in TNFR2-co-stimulated tTregs (Figure 5A). Tregs reportedly remain functional in the low-glucose microenvironment of glycolytic tumors by switching to lactate as a nutrient source<sup>47,48</sup> and rely on the solute carrier (SLC) 16 family member SLC16A1 (MCT1), a lactate importer,<sup>49</sup> to support their function.<sup>48</sup> SLC16A1 was specifically upregulated in tTregs after TNFR2 co-stimulation at the transcriptional level (Figure 5A). Protein levels of SLC16A1 were also higher in activated tTregs as compared to Tconvs, while Tconvs had higher protein levels of the lactate exporter SLC16A3 (MCT4), as well as the FA importers SLC27A2 (FATP2) and SLC27A4 (FATP4)<sup>50</sup> (Figure 5B). We therefore considered that tTregs can use lactate-derived carbon for *de novo* lipid biosynthesis when glucose availability is limited.

To test this hypothesis, we performed  $^{13}\text{C}$ -tracing of extracellular lactate in tTregs that were stimulated in medium containing low glucose (1 mM) and high [U- $^{13}\text{C}_3$ ]-L-lactate (20 mM) levels.

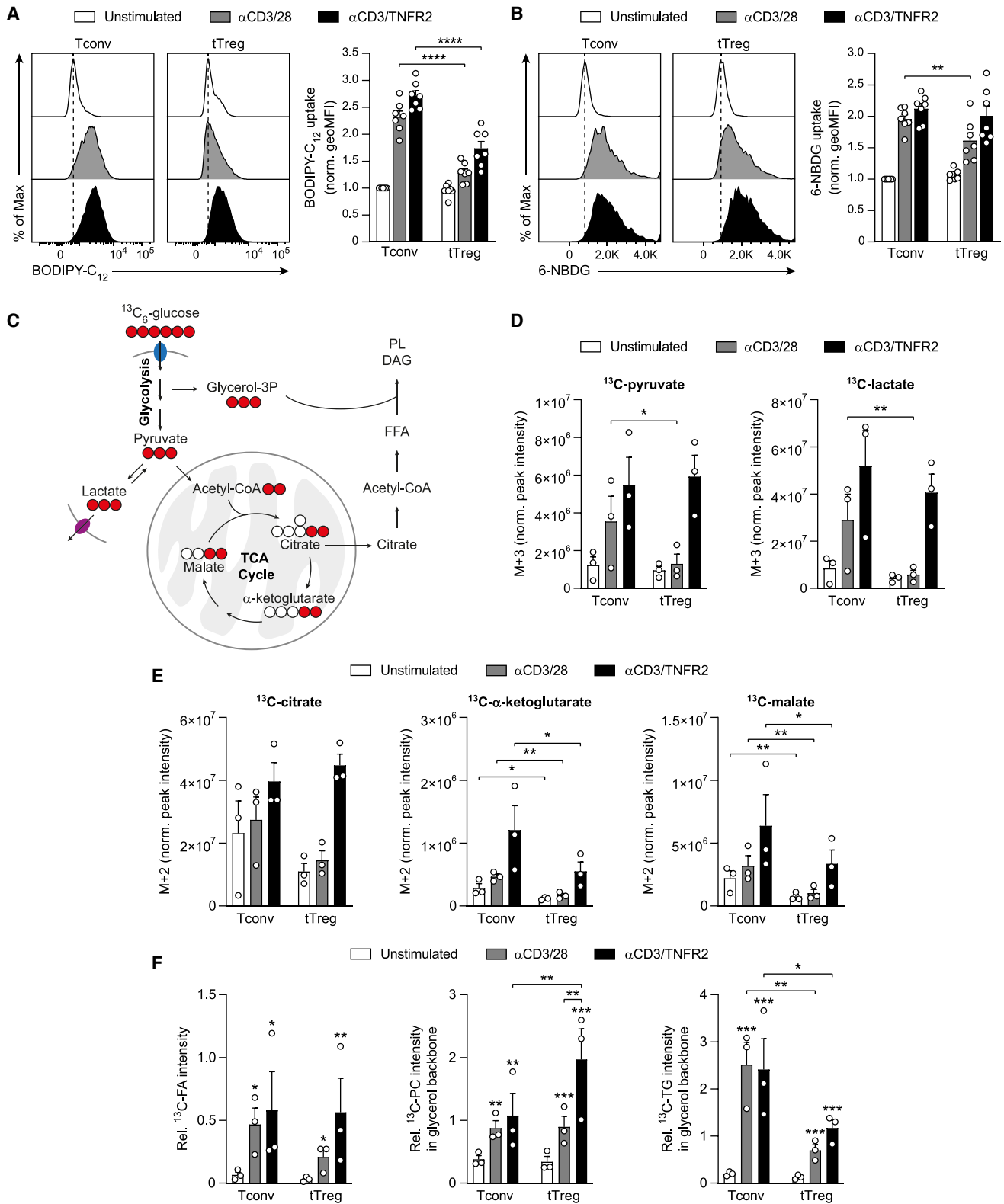
Lactate can be converted intracellularly to pyruvate by lactate dehydrogenase (LDH), which can enter into the TCA cycle and via citrate be incorporated into lipids (Figure 5C). Both cell types showed comparable  $^{13}\text{C}$ -labeling of citrate and  $\alpha$ -ketoglutarate, indicating that they can both use extracellular lactate to maintain TCA cycle activity (Figure 5D). We next measured incorporation of lactate-derived  $^{13}\text{C}$  into palmitate. Interestingly, tTregs, but not Tconvs, increased lactate-derived  $^{13}\text{C}$ -incorporation into palmitate upon activation, regardless of the co-stimulus (Figures 5E and S7).  $^{13}\text{C}$ -labeling of cholesterol was negligible. Finally, we performed isotopomer spectral analysis<sup>52</sup> using the FAMetA algorithm<sup>51</sup> to estimate *de novo* FAS (S) and exogenous FA import (I) in tTregs and Tconvs from the [U- $^{13}\text{C}_3$ ]-L-lactate tracer dataset. This model estimates the *de novo* biosynthesis rate, based on cumulative levels of  $^{13}\text{C}$ -labeled palmitate derived from [U- $^{13}\text{C}_3$ ]-L-lactate and unlabeled palmitate, derived from palmitate import or *de novo* biosynthesis from, for example, unlabeled glucose or glutamine (Figure 5F). This analysis revealed that under low-glucose and high-lactate conditions, activated tTregs use lactate to increase *de novo* palmitate synthesis, while reducing palmitate import (Figure 5G). In contrast, lactate-fueled Tconvs maintained similar *de novo* FAS and palmitate import rates following their activation (Figure 5G). These data indicate that upon activation, tTregs, but not Tconvs, can increase their ability to use lactate as a source for *de novo* FAS when glucose availability is limited.

### tTregs specifically rely on glucose/lactate-fueled FAS for proliferation

Cytosolic acetyl-CoA derived from citrate can be used for the biosynthesis of both cholesterol and FA (Figure 5C). Since in activated tTregs, glucose- and lactate-derived  $^{13}\text{C}$  was detected in palmitate, but not in cholesterol, we focused on the relevance of *de novo* FAS for tTreg function, using the small-molecule inhibitor C75 that irreversibly inhibits FA synthase (FASN) (Figure 5C). tTregs depended more on FAS for their proliferation than Tconvs, after both CD28 and TNFR2 co-stimulation (Figures 6A and 6B). C75 reduced cell viability only at higher doses than those used in the proliferation assay (Figure S8A). These data were confirmed in freshly isolated tTregs and Tconvs (Figure S8B), and by using TOFA, an inhibitor of acetyl-CoA

### Figure 3. TNFR2 co-stimulation boosts lipid synthesis in tTregs at the transcriptional level

- (A) PCA plot of transcriptomic analysis of tTregs and Tconvs stimulated as indicated.
- (B) GSEA showing the top 15 upregulated pathways in tTregs upon CD3/TNFR2 stimulation compared to CD3 stimulation alone using curated sets of genes regulating metabolism according to KEGG and Reactome databases. FDR, false discovery rate; NES, normalized enrichment score.
- (C) The top 15 predicted upstream transcriptional regulators according to IPA of the transcriptomes of tTregs after CD3/TNFR2 stimulation versus CD3 stimulation alone.
- (D) SREBF1 and SREBF2 transcript levels derived from the transcriptome data of tTregs and Tconvs stimulated as indicated, expressed as trimmed mean of M values normalized read counts. Two-way ANOVA with Tukey's post hoc test was used for statistical analysis. Data are represented as mean  $\pm$  SEM. \* $p < 0.05$ ; \*\* $p < 0.01$ .
- (E) STRING network analysis of transcriptome data showing significant up- and downregulation of SREBP target genes depicted as  $\log_2$  fold change in expression in tTregs after CD3/TNFR2 stimulation compared to CD3 stimulation alone.
- (F) Heatmap showing transcripts of molecules involved in lipid biosynthesis and degradation in tTregs activated as indicated. Z scores are color-coded.
- (G) GSEA plot showing enrichment of the TNFR2-induced gene signature in tTregs in a published tumor Treg transcriptome.<sup>42</sup> FDR  $< 0.01$ .
- (H) Comparison of  $\log_2$  fold changes in the expression of FAS-associated genes in CD3/TNFR2-activated tTregs, with tumor Tregs published by Lim et al.<sup>42</sup> Dashed lines:  $\log_2$  fold change  $\pm 0.58$ .
- (A–F) Data represent  $n = 3$  samples from individual donors in independent cultures. See also Figure S5.



(legend on next page)

carboxylase (ACC), that generates the palmitate precursor malonyl-CoA (Figures 5C and S9).

We next examined whether tTregs also relied on FAS for their proliferation under low-glucose, high-lactate conditions. Exchange of glucose by lactate did not affect the proliferation of tTregs, while it impaired the proliferative capacity of Tconvs, under either co-stimulatory condition (Figures 6C and 6D). Blockade of FASN by C75 almost completely abrogated tTreg proliferation under high-lactate conditions (Figures 6C and 6D). These data indicate that under the tested conditions, tTregs can effectively use either glucose or lactate as a nutrient and depend on their ability to synthesize FA for proliferation. Tconvs, however, prefer glucose over lactate as a nutrient and are much less reliant on FAS for their proliferation, which is consistent with their superior ability to import exogenous FA (Figure 4A).

#### tTregs rely on FAS for their suppressive activity

We next tested whether tTregs relied on FAS for their suppressive function in suppression assays. We therefore downregulated FASN in tTregs by genetic interference with a validated shRNA construct (Figures S10A and S10B) and found that this impaired the suppressive activity of tTregs (Figure 7A). Thus, tTregs rely on FAS for their proliferation and suppressive function.

Our lipidomic analysis indicated that the FA species present in tTregs are more unsaturated than in Tconvs (Figures 2A and 2B). Palmitate synthesized by FASN serves as a substrate for the enzyme stearoyl-CoA desaturase 1 (SCD1) that converts it into monounsaturated FA (MUFA), which serves as a precursor for various cellular lipids (Figure 5C). To address whether the biosynthesis of unsaturated FA is important for the suppressive function of tTregs, we downregulated SCD1 by a validated small hairpin RNA (shRNA) construct (Figure S10B). The suppressive activity of tTregs was impaired upon SCD1 knockdown (Figure 7B), showing that the biosynthesis of unsaturated FA is important for the suppressive function of tTregs. In tTregs expressing either FASN or SCD1 shRNA, the loss of suppressive function coincided with reduced expression of FOXP3 and CTLA4, which are important for tTreg identity and function (Figures S10C and S10D).

Finally, deliberate overexpression of the lactate exporter SLC16A3/MCT4 also compromised the suppressive activity of TNFR2-co-stimulated tTregs (Figures 7C, S10E, and S10F), indicating that glycolytic tTregs rely on intracellular lactate retention<sup>30</sup> to exert their suppressive function, most likely via fueling

FAS. These data demonstrate that for their suppressive function, tTregs rely on their ability to synthesize unsaturated FA.

#### DISCUSSION

TNFR2 rather than CD28 boosts glycolysis in tTregs<sup>30</sup> and, as we show here, a lipogenic program. CD3 and CD28 signal via associated tyrosine kinases and the transmembrane adaptor LAT to activate multiple signaling pathways, including the PI3 kinase-mammalian target of rapamycin (mTOR) pathway.<sup>53</sup> Co-stimulatory TNF receptor family members use a different mode of signaling and link via TRAF adaptor molecules to the NF- $\kappa$ B and Jun kinase pathways.<sup>54</sup> The glycolytic switch mediated by TNFR2 co-stimulation in CD3-activated tTregs,<sup>30,43</sup> as well as by CD28 co-stimulation in Tconvs relies on mTOR complex (mTORC) signaling.<sup>55,56</sup> It is not known how TNF receptor family members link to mTORC1, but they may feed into the CD3/CD28 signaling pathway via SHP-1, as recently described for TNFRSF7 (CD27).<sup>57</sup> Alternatively, TNF- $\alpha$  was recently found to signal to Akt through the tyrosine kinase ITK in CD4<sup>+</sup> Tconvs.<sup>58</sup> As TNFR2 can bind to TNF- $\alpha$ , similar signaling events may also occur downstream of TNFR2 engagement in tTregs. The mTOR pathway generally couples nutrient availability to the biosynthetic pathways required for cellular responses.<sup>59</sup> Our transcriptome analysis revealed that TNFR2-stimulated effector tTregs exhibit a lipogenic gene expression profile, characterized by the high expression of key enzymes involved in FA and cholesterol biosynthesis. SREBF1 and -2 were identified by enrichment analysis as upstream transcriptional regulators, in line with their key role in regulating *de novo* lipid biosynthesis.<sup>44</sup> Since mTORC1 couples to SREBF transcription factors,<sup>60,61</sup> it is likely that downstream of TNFR2, the mTORC1-SREBP signaling axis supports the lipogenic program. It has been established in mice that effector Tregs require mTORC1 signaling for *in vivo* function, at least in part because it promotes a lipogenic program.<sup>42,62</sup> These data support our finding that TNFR2-driven effector tTregs, which resemble NLT-resident Tregs,<sup>29</sup> rely on *de novo* FAS.

We found that activated Tconvs incorporated glucose-derived carbon in FA regardless of the co-stimulus, but tTregs only did so after TNFR2 co-stimulation. These tTregs did not show increased incorporation of glucose-derived carbon in cholesterol, suggesting that the mevalonate pathway, of which cholesterol is the final product, may instead generate molecules such as farnesyl- and geranylgeranyl-pyrophosphate that serve posttranslational protein modification.<sup>63</sup> Uptake activity

#### Figure 4. Glucose fuels lipid biosynthesis in TNFR2-costimulated tTregs

(A) Assessment of BODIPY-C<sub>12</sub> uptake in tTregs and Tconvs stimulated as indicated (*n* = 7).

(B) Analysis of 6-NBDG uptake in tTregs and Tconvs stimulated as indicated for 24 h (*n* = 7).

(A and B) two-way ANOVA with Tukey's post hoc test was used for statistical analysis.

(C) Scheme showing tracing of exogenous [U-<sup>13</sup>C<sub>6</sub>]-glucose-derived <sup>13</sup>C through metabolic pathways coupling glucose to *de novo* lipid biosynthesis. Red circles: <sup>13</sup>C, white circles: <sup>12</sup>C. DAG, diacylglycerol; FFA, free fatty acid; P, phosphate; PL, phospholipids.

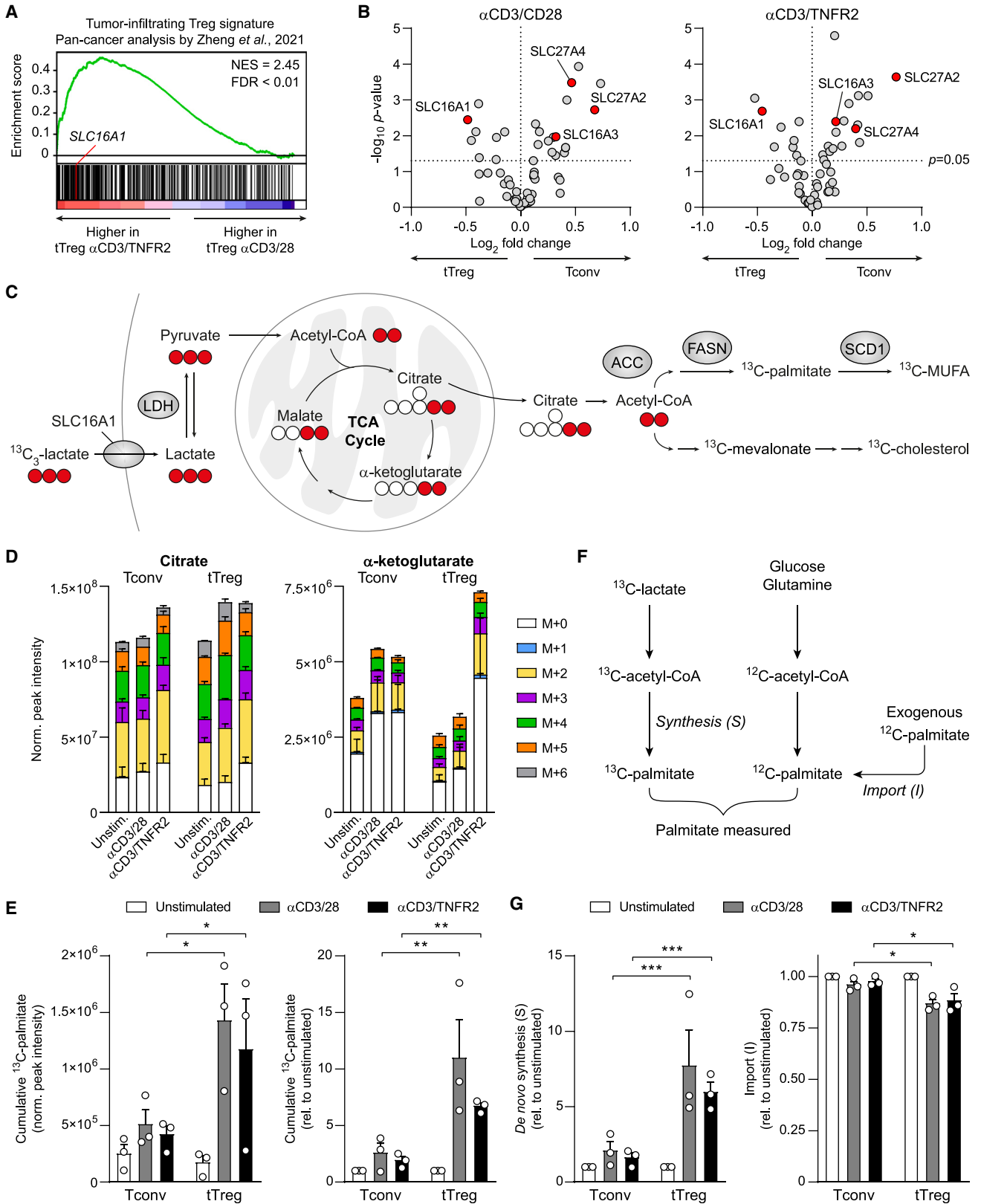
(D and E) Intracellular levels of <sup>13</sup>C-labeled glycolysis (D) and TCA cycle (E) intermediates in tTregs and Tconvs stimulated as indicated in the presence of [U-<sup>13</sup>C<sub>6</sub>]-glucose (*n* = 3). *M* indicates monoisotope metabolite mass, increased by one for each <sup>13</sup>C being incorporated.

(F) Intracellular levels of <sup>13</sup>C in FA or the glycerol backbone of PC or TG in Tconvs and tTregs stimulated as indicated in the presence of [U-<sup>13</sup>C<sub>6</sub>]-glucose.

(D–F) two-way ANOVA with Bonferroni's post hoc test was used for statistical analysis (\**p* < 0.05; \*\**p* < 0.01; \*\*\**p* < 0.001; \*\*\*\**p* < 0.0001).

(A), (B), and (D–F) Data are represented as mean  $\pm$  SEM; *n* represents samples from individual donors in independent cultures.

See also Figure S6.



(legend on next page)

of exogenous FA and expression of FA transporters (SLC27A2 and -A4) were higher in Tconvs than in tTregs, supporting the idea that tTregs are geared toward FAS rather than FA uptake. This fact predicts that Tconvs can use exogenous FA if *de novo* FAS from glucose is hampered, but tTregs cannot. Accordingly, we discovered a differential vulnerability of tTregs and Tconvs to the inhibition of the enzymes ACC and FASN that together catalyze palmitate synthesis from acetyl-CoA. ACC or FASN inhibition impaired tTreg proliferation, while Tconvs were not impacted. In addition, genetic FASN downregulation impaired the suppressive function of tTregs. Our data tie in with recent studies in mice showing that Treg expansion within tumors requires glycolysis-driven lipid biosynthesis.<sup>64</sup> Treg-specific deletion of *HMGCR*,<sup>65</sup> *Scap*, or *Fasn*<sup>42</sup> was found to provoke robust antitumor immunity, in agreement with a requirement of these lipid biosynthesis enzymes for Treg suppressive function.

The capability of tTregs to metabolize different nutrients, such as glucose and lactate, endows them with flexibility in metabolically challenging contexts like the tumor microenvironment.<sup>48</sup> Metabolic adaptation may also occur in other lactate-rich environments, such as the skeletal muscle, where Tregs play an important role in tissue regeneration.<sup>66</sup> Classically, lactate is considered to be a waste product of glycolysis.<sup>67</sup> However, it can also be oxidized to pyruvate and serve as a carbon source for the TCA cycle.<sup>68</sup> We show here that human tTregs express the lactate importer SLC16A1 at higher levels and the lactate exporter SLC16A3 at lower levels than Tconvs, which agrees with our earlier finding that glycolytic tTregs accumulate more intracellular lactate than glycolytic Tconvs.<sup>30</sup> Under low-glucose conditions, lactate proved to be an alternative nutrient for human tTregs, while Tconvs failed to thrive on it. Under high-lactate and low-glucose conditions, both CD28 and TNFR2 co-stimulation increased FAS in tTregs in equal measure. This can be explained by the fact that lactate feeds into the TCA cycle downstream of the glycolysis pathway that is selectively boosted in tTregs by TNFR2 co-stimulation. In agreement with a prominent role for lactate as a nutrient for tTregs, murine Tregs deficient for lactate importer *Slc16a1* displayed impaired suppressive function *in vivo*.<sup>48</sup> Moreover, a key study showed that Tregs are naturally geared toward using lactate as a nutrient to support their proliferation, survival, and suppressive function under low-glucose

conditions.<sup>47</sup> We demonstrate here that lactate can fuel *de novo* FAS in both tTregs and Tconvs, but that tTregs are uniquely reliant on this pathway for their proliferation when glucose availability is limited. This specific vulnerability of tTregs may explain why Treg-specific loss of FASN in a mouse model led to reduced tumor growth.<sup>42</sup> Possibly, Tconvs were released from Treg-mediated suppression and cleared the tumor. We conclude that effector tTregs, as found in healthy and diseased tissues, likely rely on *de novo* FA and lipid biosynthesis for their proliferation and function and can effectively use either glucose or lactate to sustain this metabolic program.

Next to glucose and glutamine, FA are generally listed as nutrients for diverse cell types. Long-chain free FA can be imported into cells via diverse transporters and broken down into acetyl-CoA by the FA oxidation (FAO) pathway. Early studies reported that Tregs exhibit increased FAO compared to Tconvs.<sup>69,70</sup> Also, one study argues that T helper 17-type Tconvs, but not Tregs, rely on FAS,<sup>71</sup> which is in seeming contrast to our findings. However, these studies were done in *in vitro* transforming growth factor  $\beta$ -driven induced Tregs that are converted from Tconvs, which have many hallmarks that set them apart from tTregs.<sup>72</sup> The tTregs we have studied here represent the stable tTregs that populate lymphoid and non-lymphoid organs in human and mice, as we have shown previously.<sup>29</sup> Certain NLTs can also harbor pTregs that are converted from Tconvs *in vivo* and likely have properties distinct from effector tTregs. Since there are no markers to discern these populations besides TCR- or transcriptome-based lineage tracing, the literature is confusing regarding *in vivo* Treg properties. Treg-specific deletion of the FA importer CD36 driven by the *Foxp3* promoter did not cause autoimmunity and did not impair Treg maintenance or function *in vivo*,<sup>73</sup> in agreement with our finding that Tregs can use glucose and lactate as nutrients to synthesize FA *de novo*. However, in subcutaneously implanted tumors, Tregs required FA uptake and oxidation for survival and suppressive function.<sup>73</sup> Along similar lines, exogenous oleic acid was found to stimulate an FAO gene expression program in human blood-derived Tregs that could also be recognized in visceral adipose tissue-resident Tregs.<sup>74</sup> These opposing findings can be explained by nutrient availability in the corresponding contexts. Subcutaneous and visceral adipose tissue are rich in FA but may contain limited amounts of water-soluble nutrients such as glucose and lactate.

### Figure 5. tTregs but not Tconvs use lactate for FAS upon glucose deprivation

- (A) GSEA plot showing enrichment of a published pan-cancer tumor-infiltrating Treg gene signature<sup>46</sup> in the transcriptome of CD3/TNFR2-compared to CD3/28-stimulated tTregs.
- (B) Proteomics analysis comparing SLC expression in tTregs versus Tconvs stimulated as indicated. Dotted horizontal line indicates  $p = 0.05$ . SLC involved in lactate or FA transport are highlighted in red. Unpaired Student's t test with Benjamini-Krieger-Yekutieli method was used for statistical analysis; FDR < 0.05.
- (C) Scheme showing tracing of exogenous [U-<sup>13</sup>C<sub>3</sub>]-lactate-derived <sup>13</sup>C through TCA cycle and lipid biosynthesis pathways. Red circles: <sup>13</sup>C, white circles: <sup>12</sup>C.
- (D) Distribution of <sup>13</sup>C-labeled TCA cycle intermediates in Tconvs and tTregs stimulated as indicated in the presence of [U-<sup>13</sup>C<sub>3</sub>]-L-lactate. *M* indicates mono-isotope metabolite mass, increased by one for each <sup>13</sup>C being incorporated.
- (E) Cumulative <sup>13</sup>C-labeling of palmitate in tTregs and Tconvs expressed as normalized peak intensity (left) and relative increase in labeling compared to unstimulated controls (right).
- (F) Schematic overview of the origin of palmitate (<sup>12</sup>C- and <sup>13</sup>C-labeled), indicating *de novo* synthesis (S) from [U-<sup>13</sup>C<sub>3</sub>]-lactate and import (I) of exogenous <sup>12</sup>C-palmitate as main parameters to analyze FA metabolism by FAMetA.<sup>51</sup>
- (G) *De novo* FAS rate (S) and palmitate import rate (I) according to FAMetA.<sup>51</sup>
- (E and G) Two-way ANOVA with Bonferroni's post hoc test was used for statistical analysis ( $p < 0.05$ ;  $**p < 0.01$ ;  $***p < 0.001$ ). Data are represented as mean  $\pm$  SEM (A, B, D, E, G). Data represent  $n = 3$  samples from individual donors in independent cultures.
- See also Figure S7.

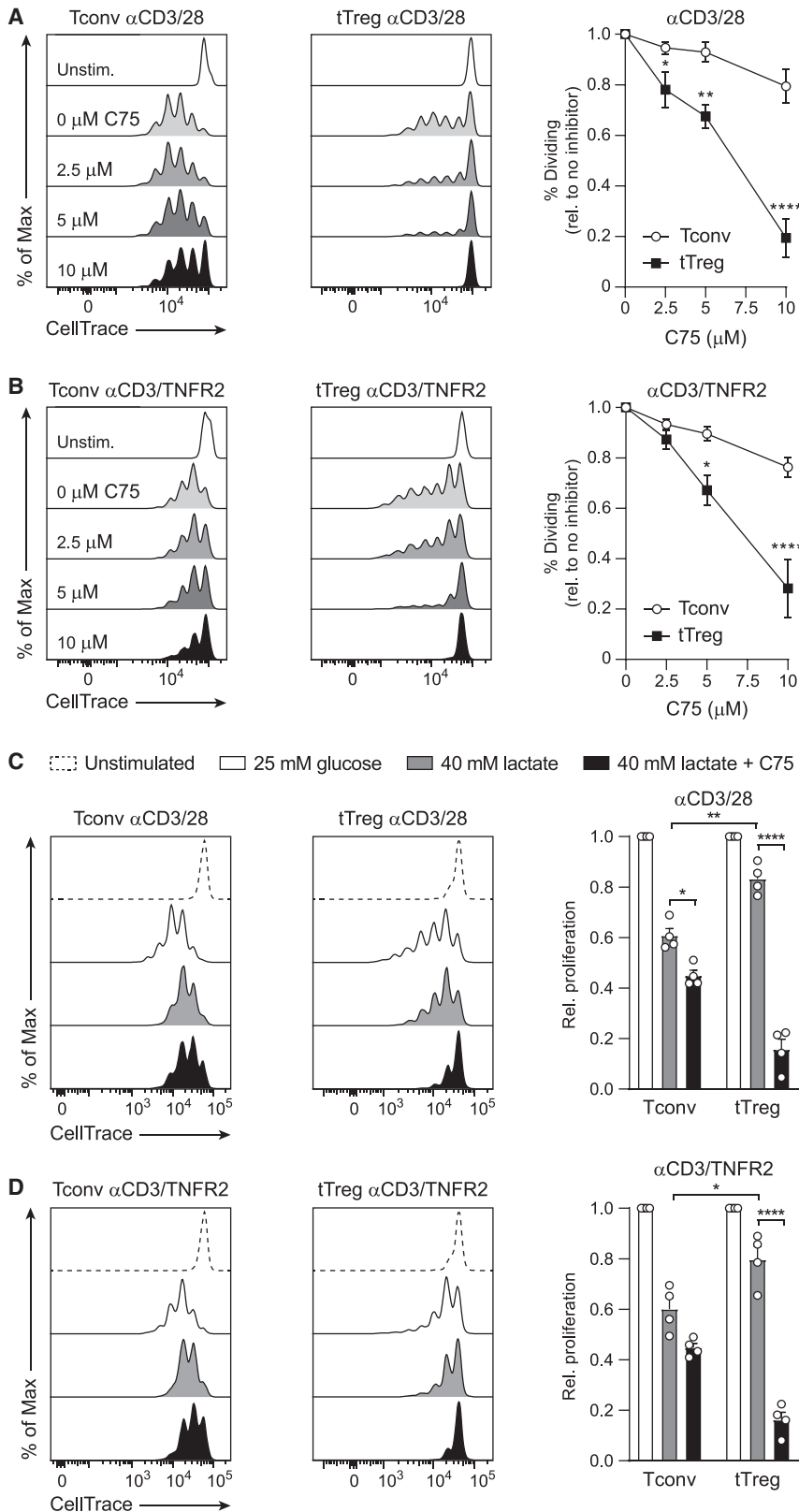


**Figure 6. tTregs specifically rely on glucose/lactate-fueled FAS for proliferation**

(A and B) tTreg and Tconv proliferation upon indicated stimulation in the presence of increasing C75 concentrations.

(C and D) Proliferation of tTregs and Tconvs upon indicated stimulation and culture conditions.

(A–D) Two-way ANOVA with Tukey's post hoc test was used for statistical analysis ( $p < 0.05$ ;  $**p < 0.01$ ;  $****p < 0.0001$ ). Data are represented as mean  $\pm$  SEM of  $n = 4$  samples from individual donors in independent cultures. See also Figures S8 and S9.

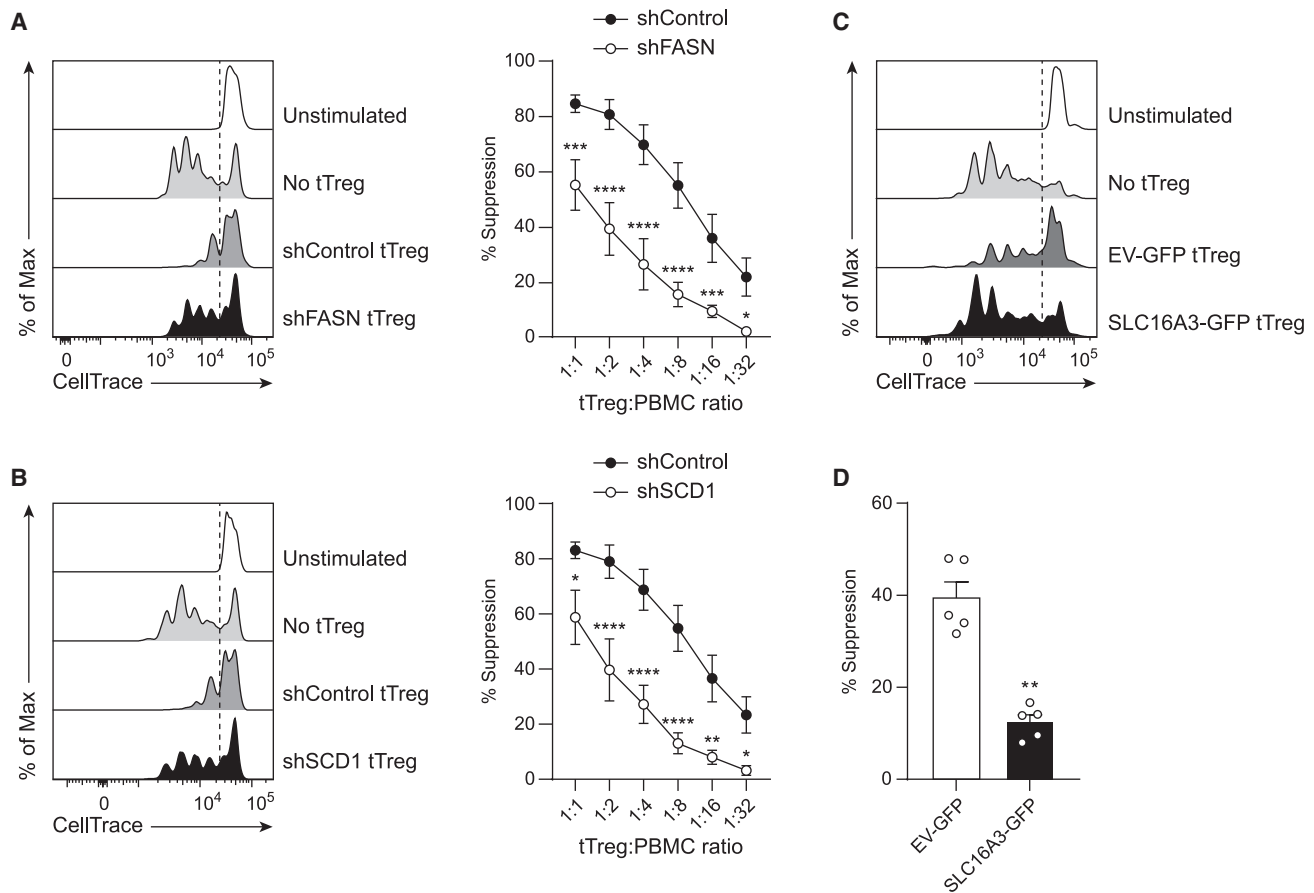


**Figure 7. tTregs rely on FAS for their suppressive activity**

(A and B) Assessment of the suppressive capacity of FASN-KD (A) or SCD1-KD (B) tTregs. Two-way ANOVA with Bonferroni's post hoc test was used for statistical analysis.

(C and D) Assessment of the suppressive capacity of tTregs with EV-GFP or SLC16A3-GFP overexpression cocultured with CellTrace-labeled PBMC in a 1:4 ratio. Paired two-sided Student's t test was used for statistical analysis.

(A–D) Data are presented as mean  $\pm$  SEM of  $n = 5$  samples from individual donors in independent cultures ( $*p < 0.05$ ;  $**p < 0.01$ ;  $***p < 0.001$ ;  $****p < 0.0001$ ). See also [Figure S10](#).

Tregs in such tissues may therefore adapt to rely on FA uptake and FAO. Overall, these data suggest that NLT-resident tTregs may adapt to tissue-specific nutrient availability for lipid biosynthesis.

Our lipidomic analysis indicated that Tconvs are richer than tTregs in neutral lipids, including (ether)-DG and (ether)-TG. Accordingly, glucose-derived carbon was preferentially used for TG synthesis in Tconvs. Our finding that tTregs have characteristically low TG levels ties in with observations in mice, where *Batf*, a transcription factor essential for NLT-resident Tregs,<sup>3</sup> suppressed TG synthesis.<sup>75</sup> Deletion of *Batf* in Tregs impaired their suppressive function, in part due to elevated TG abundance, as shown by the inhibition of TG synthetase *Dgat2*. High TG content in pro-inflammatory Tconvs and high phospholipid content in anti-inflammatory tTregs provide an interesting analogy with pro-inflammatory M1 macrophages that incorporate exogenous FA into TG and anti-inflammatory M2 macrophages that incorporate them into phospholipids.<sup>76,77</sup> TG are stored in lipid droplets, from where they can be mobilized for

eicosanoid synthesis<sup>78</sup> and drive inflammatory responses, as observed in macrophages,<sup>76,79,80</sup> neutrophils,<sup>81,82</sup> mast cells,<sup>83,84</sup> microglia,<sup>85</sup> and innate lymphoid cells.<sup>86</sup> Moreover, pro-inflammatory CD4<sup>+</sup> T cells from rheumatoid arthritis patients were also found to accumulate lipid droplets.<sup>87</sup>

The physicochemical properties of cellular membranes are determined by FA content, length, and saturation.<sup>88</sup> We found that tTregs make discerning phospholipids and TG with long and unsaturated FA chains, which is boosted by TNFR2 co-stimulation and required for their suppressive function, as shown by the knockdown of SCD1, a desaturase that introduces a double bond at the  $\Delta 9$  position. TNFR2 co-stimulation also upregulated *FADS1* and *FADS2*,  $\Delta 5$ - and  $\Delta 6$ -desaturases, respectively, which are rate limiting in the synthesis of polyunsaturated FA (PUFA). Membrane lipid composition can impact T cell function in a variety of ways. Lipid species with saturated FA lead to tighter packing and lower membrane fluidity, while unsaturated FAs enable lower membrane order with higher flexibility and fluidity.<sup>88</sup> In line with our observation that Tregs have a high unsaturated

FA content within phospholipid species, Tregs reportedly have a lower membrane order than Tconvs.<sup>89</sup> Increased membrane flexibility may serve effector tTreg shaping and motility, which is strongly increased after TNFR2 co-stimulation<sup>29</sup> and important for Treg function in tissues. It may also serve the membrane dynamics involved in CTLA4-mediated suppression of Tconvs.<sup>90</sup> Furthermore, PUFA are known to impair membrane packing at TCR signaling foci in Tconvs,<sup>33,91</sup> and therefore tTregs may have intrinsically different arrangements for transmembrane signaling than Tconvs. Further studies should reveal all functional consequences of the differential lipid compositions of tTregs and Tconvs and the underlying cell biological mechanisms. However, of immediate clinical relevance is our finding that tTregs, but not Tconvs, have the capacity to switch to lactate-fueled FAS under low-glucose conditions, which is a tTreg-specific vulnerability that can be therapeutically exploited.

### Limitations of the study

The difference in lipid composition between tTregs and Tconvs influences receptor proximal signaling events, for example, by impact on receptor clustering in membrane microdomains and recruitment of signaling molecules to the plasma membrane. This can be examined by various approaches, such as characterization of lipid rafts coupled to mapping of intracellular signaling events by unbiased phosphoproteomics approaches. We could not rescue the effects of FAS inhibition in tTregs by adding exogenous palmitate, which may be explained by the fact that this predominantly leads to lipid droplet formation.<sup>92</sup> It should therefore be tested whether ablation of FAS-associated enzymes in tTregs alters their lipidome, which in combination with the aforementioned biochemical studies could provide a direct link between lipidome remodeling and tTreg function.

Regarding *in vivo* relevance, here, we show by comparative transcriptomics analyses that high *SLC16A1* expression on TNFR2-co-stimulated tTregs is a hallmark of tumor Tregs. Likewise, TNFR2-co-stimulated and tumor Tregs showed increased expression of FAS-associated genes, particularly those involved in FA desaturation. Although a reductionist *in vitro* approach as adopted in our study can reveal novel mechanistic insights that are complementary to *in vivo* studies, approaches like *in vivo* isotopologue tracing<sup>93,94</sup> coupled to lipidome analysis will be important to provide a definitive relationship between lipid biosynthesis and Treg function in, for instance, cancer, inflammation, or tissue repair.

### RESOURCE AVAILABILITY

#### Lead contact

Further information and requests for resources and reagents should be directed to and will be fulfilled by the lead contact, Sander de Kivit ([s.de\\_kivit@lumc.nl](mailto:s.de_kivit@lumc.nl)).

#### Materials availability

This study did not generate new unique reagents.

#### Data and code availability

- RNA-seq data have been deposited at GEO and are publicly available under the accession number GSE138604. Proteomics data have been deposited to the ProteomeXchange Consortium (<http://>

[proteomecentral.proteomexchange.org](http://proteomecentral.proteomexchange.org)) via the PRIDE repository<sup>95</sup> with the dataset identifier PXD048504.

- This paper does not report original code.
- Any additional information required to reanalyze the data reported in this paper is available from the [lead contact](#) upon request.

### ACKNOWLEDGMENTS

We thank George M.C. Janssen, Rayman T.N. Tjokrodjirjo, and Peter A. van Veelen from the Center for Proteomics and Metabolomics at Leiden University Medical Center for performing proteomics and the personnel of the Flow Cytometry Facility at Leiden University Medical Center for technical assistance. We acknowledge [BioRender.com](#), which we used for creating the graphical abstract. This work was supported by subgrant IC100025 of the Institute for Chemical Immunology, funded by ZonMW Gravitation to J.B. and C.R.B., and by a grant from the Oncode Institute to J.B. M.G. was partially supported by NWO XOmics project no. 184.034.019.

### AUTHOR CONTRIBUTIONS

Conceptualization, S.d.K., M.M., S.K., E.A.Z., C.R.B., M.G., and J.B.; methodology, S.d.K., M.M., S.K., E.A.Z., M.H., C.R.B., M.G., and J.B.; investigation, S.d.K., M.M., S.K., R.J.E.D., E.A.Z., M.H., L.J.V., E.d.V., E.S., and N.B.; formal analysis, S.d.K., M.M., S.K., R.J.E.D., E.A.Z., and L.J.V.; writing – original draft, S.d.K., M.M., and J.B.; writing – review & editing, S.K., R.J.E.D., E.A.Z., C.R.B., and M.G.; visualization, S.d.K., M.M., S.K., R.J.E.D., and E.A.Z.; supervision, S.d.K., S.K., C.R.B., M.G., and J.B.; funding acquisition, C.R.B., M.G., and J.B.

### DECLARATION OF INTERESTS

The authors declare no competing interests.

### STAR★METHODS

Detailed methods are provided in the online version of this paper and include the following:

- KEY RESOURCES TABLE
- EXPERIMENTAL MODEL AND STUDY PARTICIPANT DETAILS
  - Human material
- METHOD DETAILS
  - T cell isolation and sorting
  - T cell expansion and restimulation
  - Flow cytometry
  - Lipidomics
  - Transcriptomics
  - Glucose and FA uptake assay
  - <sup>13</sup>C stable-isotope tracing
  - Neutral lipid staining by flow cytometry
  - T cell proliferation
  - T cell transductions
  - Western blot
  - Suppression assay
  - Proteomics
- QUANTIFICATION AND STATISTICAL ANALYSIS
- ADDITIONAL RESOURCES

### SUPPLEMENTAL INFORMATION

Supplemental information can be found online at <https://doi.org/10.1016/j.celrep.2024.114681>.

Received: March 18, 2024

Revised: July 10, 2024

Accepted: August 8, 2024

Published: August 23, 2024

REFERENCES

- Dikiy, S., and Rudensky, A.Y. (2023). Principles of regulatory T cell function. *Immunity* 56, 240–255. <https://doi.org/10.1016/j.immuni.2023.01.004>.
- Panduro, M., Benoist, C., and Mathis, D. (2016). Tissue Tregs. *Annu. Rev. Immunol.* 34, 609–633. <https://doi.org/10.1146/annurev-immunol-032712-095948>.
- Delacher, M., Simon, M., Sanderink, L., Hotz-Wagenblatt, A., Wuttke, M., Schambeck, K., Schmideitner, L., Bittner, S., Pant, A., Ritter, U., et al. (2021). Single-cell chromatin accessibility landscape identifies tissue repair program in human regulatory T cells. *Immunity* 54, 702–720.e17. <https://doi.org/10.1016/j.immuni.2021.03.007>.
- Raffin, C., Vo, L.T., and Bluestone, J.A. (2020). Treg cell-based therapies: challenges and perspectives. *Nat. Rev. Immunol.* 20, 158–172. <https://doi.org/10.1038/s41577-019-0232-6>.
- Tanaka, A., and Sakaguchi, S. (2017). Regulatory T cells in cancer immunotherapy. *Cell Res.* 27, 109–118. <https://doi.org/10.1038/cr.2016.151>.
- Plitas, G., and Rudensky, A.Y. (2020). Regulatory T Cells in Cancer. *Annu. Rev. Canc Biol* 4, 459–477. <https://doi.org/10.1146/annurev-cancerbio-030419-033428>.
- Savage, P.A., Klawon, D.E.J., and Miller, C.H. (2020). Regulatory T Cell Development. *Annu. Rev. Immunol.* 38, 421–453. <https://doi.org/10.1146/annurev-immunol-100219-020937>.
- Burton, O.T., Bricard, O., Tareen, S., Gergelits, V., Andrews, S., Biggins, L., Roca, C.P., Whyte, C., Junius, S., Brajic, A., et al. (2024). The tissue-resident regulatory T cell pool is shaped by transient multi-tissue migration and a conserved residency program. *Immunity* 57, 1586–1602.e10. <https://doi.org/10.1016/j.immuni.2024.05.023>.
- Fontenot, J.D., Gavin, M.A., and Rudensky, A.Y. (2003). Foxp3 programs the development and function of CD4+CD25+ regulatory T cells. *Nat. Immunol.* 4, 330–336. <https://doi.org/10.1038/ni904>.
- Hori, S., Nomura, T., and Sakaguchi, S. (2003). Control of regulatory T cell development by the transcription factor Foxp3. *Science* 299, 1057–1061. <https://doi.org/10.1126/science.1079490>.
- Bennett, C.L., Christie, J., Ramsdell, F., Brunkow, M.E., Ferguson, P.J., Whitesell, L., Kelly, T.E., Saulsbury, F.T., Chance, P.F., and Ochs, H.D. (2001). The immune dysregulation, polyendocrinopathy, enteropathy, X-linked syndrome (IPEX) is caused by mutations of FOXP3. *Nat. Genet.* 27, 20–21. <https://doi.org/10.1038/83713>.
- Wildin, R.S., Ramsdell, F., Peake, J., Faravelli, F., Casanova, J.L., Buist, N., Levy-Lahad, E., Mazzella, M., Goulet, O., Perroni, L., et al. (2001). X-linked neonatal diabetes mellitus, enteropathy and endocrinopathy syndrome is the human equivalent of mouse scurfy. *Nat. Genet.* 27, 18–20. <https://doi.org/10.1038/83707>.
- Josefowicz, S.Z., Lu, L.F., and Rudensky, A.Y. (2012). Regulatory T cells: mechanisms of differentiation and function. *Annu. Rev. Immunol.* 30, 531–564. <https://doi.org/10.1146/annurev-immunol.25.022106.141623>.
- Liston, A., and Gray, D.H.D. (2014). Homeostatic control of regulatory T cell diversity. *Nat. Rev. Immunol.* 14, 154–165. <https://doi.org/10.1038/nri3605>.
- Trujillo-Ochoa, J.L., Kazemian, M., and Afzali, B. (2023). The role of transcription factors in shaping regulatory T cell identity. *Nat. Rev. Immunol.* 23, 842–856. <https://doi.org/10.1038/s41577-023-00893-7>.
- Ferraro, A., D’Alise, A.M., Raj, T., Asinovski, N., Phillips, R., Ergun, A., Replogle, J.M., Bernier, A., Laffel, L., Stranger, B.E., et al. (2014). Interindividual variation in human T regulatory cells. *Proc. Natl. Acad. Sci. USA* 111, E1111–E1120. <https://doi.org/10.1073/pnas.1401343111>.
- Feuerer, M., Hill, J.A., Mathis, D., and Benoist, C. (2009). Foxp3+ regulatory T cells: differentiation, specification, subphenotypes. *Nat. Immunol.* 10, 689–695. <https://doi.org/10.1038/ni.1760>.
- Miyara, M., Yoshioka, Y., Kitoh, A., Shima, T., Wing, K., Niwa, A., Parizot, C., Taffin, C., Heike, T., Valeyre, D., et al. (2009). Functional Delineation and Differentiation Dynamics of Human CD4+ T Cells Expressing the FoxP3 Transcription Factor. *Immunity* 30, 899–911. <https://doi.org/10.1016/j.immuni.2009.03.019>.
- Schmidl, C., Hansmann, L., Lassmann, T., Balwier, P.J., Kawaji, H., Itoh, M., Kawai, J., Nagao-Sato, S., Suzuki, H., Andreesen, R., et al. (2014). The enhancer and promoter landscape of human regulatory and conventional T-cell subpopulations. *Blood* 123, e68–e78. <https://doi.org/10.1182/blood-2013-02-486944>.
- Cuadrado, E., van den Biggelaar, M., de Kivit, S., Chen, Y.Y., Slot, M., Doubal, I., Meijer, A., van Lier, R.A.W., Borst, J., and Amsen, D. (2018). Proteomic Analyses of Human Regulatory T Cells Reveal Adaptations in Signaling Pathways that Protect Cellular Identity. *Immunity* 48, 1046–1059.e6. <https://doi.org/10.1016/j.immuni.2018.04.008>.
- Rieckmann, J.C., Geiger, R., Hornburg, D., Wolf, T., Kveler, K., Jarrossay, D., Sallusto, F., Shen-Orr, S.S., Lanzavecchia, A., Mann, M., and Meissner, F. (2017). Social network architecture of human immune cells unveiled by quantitative proteomics. *Nat. Immunol.* 18, 583–593. <https://doi.org/10.1038/ni.3693>.
- Zemmour, D., Zilionis, R., Kiner, E., Klein, A.M., Mathis, D., and Benoist, C. (2018). Single-cell gene expression reveals a landscape of regulatory T cell phenotypes shaped by the TCR. *Nat. Immunol.* 19, 291–301. <https://doi.org/10.1038/s41590-018-0051-0>.
- Lubrano di Ricco, M., Ronin, E., Collares, D., Divoux, J., Grégoire, S., Wajant, H., Gomes, T., Grinberg-Bleyer, Y., Baud, V., Marodon, G., and Salomon, B.L. (2020). Tumor necrosis factor receptor family costimulation increases regulatory T-cell activation and function via NF-κB. *Eur. J. Immunol.* 50, 972–985. <https://doi.org/10.1002/eji.201948393>.
- Rubtsov, Y.P., Niec, R.E., Josefowicz, S., Li, L., Darce, J., Mathis, D., Benoist, C., and Rudensky, A.Y. (2010). Stability of the regulatory T cell lineage in vivo. *Science* 329, 1667–1671. <https://doi.org/10.1126/science.1191996>.
- Miyao, T., Floess, S., Setoguchi, R., Luche, H., Fehling, H.J., Waldmann, H., Huehn, J., and Hori, S. (2012). Plasticity of Foxp3(+) T cells reflects promiscuous Foxp3 expression in conventional T cells but not reprogramming of regulatory T cells. *Immunity* 36, 262–275. <https://doi.org/10.1016/j.immuni.2011.12.012>.
- Rudra, D., deRoos, P., Chaudhry, A., Niec, R.E., Arvey, A., Samstein, R.M., Leslie, C., Shaffer, S.A., Goodlett, D.R., and Rudensky, A.Y. (2012). Transcription factor Foxp3 and its protein partners form a complex regulatory network. *Nat. Immunol.* 13, 1010–1019. <https://doi.org/10.1038/ni.2402>.
- Li, P., Spolski, R., Liao, W., and Leonard, W.J. (2014). Complex interactions of transcription factors in mediating cytokine biology in T cells. *Immunol. Rev.* 267, 141–156. <https://doi.org/10.1111/imr.12199>.
- Chapman, N.M., and Chi, H. (2022). Metabolic adaptation of lymphocytes in immunity and disease. *Immunity* 55, 14–30. <https://doi.org/10.1016/j.immuni.2021.12.012>.
- Mensink, M., Verleng, L.J., Schrama, E., Janssen, G.M., Tjokrodijro, R.T., van Veelen, P.A., Jiang, Q., Pascutti, M.F., van der Hoorn, M.L., Eikmans, M., et al. (2024). Treg cells from human blood differentiate into non-lymphoid tissue-resident effector cells upon TNFR2 costimulation. *JCI Insight* 9, e172942. <https://doi.org/10.1172/jci.insight.172942>.
- de Kivit, S., Mensink, M., Hoekstra, A.T., Berlin, I., Derks, R.J.E., Both, D., Aslam, M.A., Amsen, D., Berkens, C.R., and Borst, J. (2020). Stable human regulatory T cells switch to glycolysis following TNF receptor 2 costimulation. *Nat. Metab.* 2, 1046–1061. <https://doi.org/10.1038/s42255-020-00271-w>.
- D’Angelo, G., and La Manno, G. (2023). The lipotype hypothesis. *Nat. Rev. Mol. Cell Biol.* 24, 1–2. <https://doi.org/10.1038/s41580-022-00556-w>.
- Tavano, R., Contento, R.L., Baranda, S.J., Soligo, M., Tuosto, L., Manes, S., and Viola, A. (2006). CD28 interaction with filamin-A controls lipid raft accumulation at the T-cell immunological synapse. *Nat. Cell Biol.* 8, 1270–1276. <https://doi.org/10.1038/ncb1492>.

33. Zech, T., Ejings, C.S., Gaus, K., de Wet, B., Shevchenko, A., Simons, K., and Harder, T. (2009). Accumulation of raft lipids in T-cell plasma membrane domains engaged in TCR signalling. *EMBO J.* 28, 466–476. <https://doi.org/10.1038/emboj.2009.6>.
34. Viola, A., Schroeder, S., Sakakibara, Y., and Lanzavecchia, A. (1999). T lymphocyte costimulation mediated by reorganization of membrane microdomains. *Science* 283, 680–682. <https://doi.org/10.1126/science.283.5402.680>.
35. Cho, W., and Stahelin, R.V. (2005). Membrane-protein interactions in cell signaling and membrane trafficking. *Annu. Rev. Biophys. Biomol. Struct.* 34, 119–151. <https://doi.org/10.1146/annurev.biophys.33.110502.133337>.
36. Cipolletta, D., Feuerer, M., Li, A., Kamei, N., Lee, J., Shoelson, S.E., Benoist, C., and Mathis, D. (2012). PPAR- $\gamma$  is a major driver of the accumulation and phenotype of adipose tissue Treg cells. *Nature* 486, 549–553. <https://doi.org/10.1038/nature11132>.
37. Bensinger, S.J., Bradley, M.N., Joseph, S.B., Zelcer, N., Janssen, E.M., Hausner, M.A., Shih, R., Parks, J.S., Edwards, P.A., Jamieson, B.D., and Tontonoz, P. (2008). LXR signaling couples sterol metabolism to proliferation in the acquired immune response. *Cell* 134, 97–111. <https://doi.org/10.1016/j.cell.2008.04.052>.
38. O'Neill, L.A.J., Kishton, R.J., and Rathmell, J. (2016). A guide to immunometabolism for immunologists. *Nat. Rev. Immunol.* 16, 553–565. <https://doi.org/10.1038/nri.2016.70>.
39. Opstelten, R., de Kivit, S., Slot, M.C., van den Biggelaar, M., Iwaszkiewicz-Grzes, D., Gliwiński, M., Scott, A.M., Blom, B., Trzonkowski, P., Borst, J., et al. (2020). GPA33: A Marker to Identify Stable Human Regulatory T Cells. *J. Immunol.* 204, 3139–3148. <https://doi.org/10.4049/jimmunol.1901250>.
40. Ghorasaini, M., Tsezou, K.I., Verhoeven, A., Mohammed, Y., Vlachoyiannopoulos, P., Mikros, E., and Giera, M. (2022). Congruence and Complementarity of Differential Mobility Spectrometry and NMR Spectroscopy for Plasma Lipidomics. *Metabolites* 12, 1030. <https://doi.org/10.3390/metabo12111030>.
41. Ghorasaini, M., Mohammed, Y., Adamski, J., Bettcher, L., Bowden, J.A., Cabruja, M., Contrepolis, K., Ellenberger, M., Gajera, B., Haid, M., et al. (2021). Cross-Laboratory Standardization of Preclinical Lipidomics Using Differential Mobility Spectrometry and Multiple Reaction Monitoring. *Anal. Chem.* 93, 16369–16378. <https://doi.org/10.1021/acs.analchem.1c02826>.
42. Lim, S.A., Wei, J., Nguyen, T.L.M., Shi, H., Su, W., Palacios, G., Dhungana, Y., Chapman, N.M., Long, L., Saravia, J., et al. (2021). Lipid signaling enforces functional specialization of T<sub>reg</sub> cells in tumours. *Nature* 591, 306–311. <https://doi.org/10.1038/s41586-021-03235-6>.
43. Mensink, M., Tran, T.N.M., Zaal, E.A., Schrama, E., Berkers, C.R., Borst, J., and de Kivit, S. (2022). TNFR2 Costimulation Differentially Impacts Regulatory and Conventional CD4<sup>+</sup> T-Cell Metabolism. *Front. Immunol.* 13, 881166. <https://doi.org/10.3389/fimmu.2022.881166>.
44. Horton, J.D., Goldstein, J.L., and Brown, M.S. (2002). SREBPs: activators of the complete program of cholesterol and fatty acid synthesis in the liver. *J. Clin. Invest.* 109, 1125–1131. <https://doi.org/10.1172/Jci200215593>.
45. Menk, A.V., Scharping, N.E., Moreci, R.S., Zeng, X., Guy, C., Salvatore, S., Bae, H., Xie, J., Young, H.A., Wendell, S.G., and Delgoffe, G.M. (2018). Early TCR Signaling Induces Rapid Aerobic Glycolysis Enabling Distinct Acute T Cell Effector Functions. *Cell Rep.* 22, 1509–1521. <https://doi.org/10.1016/j.celrep.2018.01.040>.
46. Zheng, L., Qin, S., Si, W., Wang, A., Xing, B., Gao, R., Ren, X., Wang, L., Wu, X., Zhang, J., et al. (2021). Pan-cancer single-cell landscape of tumor-infiltrating T cells. *Science* 374, abe6474. <https://doi.org/10.1126/science.abe6474>.
47. Angelin, A., Gil-de-Gomez, L., Dahiya, S., Jiao, J., Guo, L., Levine, M.H., Wang, Z., Quinn, W.J., 3rd, Kopinski, P.K., Wang, L., et al. (2017). Foxp3 Reprograms T Cell Metabolism to Function in Low-Glucose, High-Lactate Environments. *Cell Metabol.* 25, 1282–1293. <https://doi.org/10.1016/j.cmet.2016.12.018>.
48. Watson, M.J., Vignali, P.D.A., Mullett, S.J., Overacre-Delgoffe, A.E., Peralta, R.M., Grebinoski, S., Menk, A.V., Rittenhouse, N.L., DePeaux, K., Whetstone, R.D., et al. (2021). Metabolic support of tumour-infiltrating regulatory T cells by lactic acid. *Nature* 591, 645–651. <https://doi.org/10.1038/s41586-020-03045-2>.
49. Bosshart, P.D., Charles, R.P., Garibisinh, R.A.A., Schlessinger, A., and Fotiadis, D. (2021). SLC16 Family: From Atomic Structure to Human Disease. *Trends Biochem. Sci.* 46, 28–40. <https://doi.org/10.1016/j.tibs.2020.07.005>.
50. He, Q., Chen, Y., Wang, Z., He, H., and Yu, P. (2023). Cellular Uptake, Metabolism and Sensing of Long-Chain Fatty Acids. *Front. Biosci.* 28, 10. <https://doi.org/10.31083/j.fb12801010>.
51. Alcoriza-Balaguer, M.I., Garcia-Canaveras, J.C., Benet, M., Juan-Vidal, O., and Lahoz, A. (2023). FAMeTA: a mass isotopologue-based tool for the comprehensive analysis of fatty acid metabolism. *Brief Bioinform* 24, bbad064. <https://doi.org/10.1093/bib/bbad064>.
52. Kelleher, J.K., and Masterson, T.M. (1992). Model equations for condensation biosynthesis using stable isotopes and radioisotopes. *Am. J. Physiol.* 262, E118–E125. <https://doi.org/10.1152/ajpendo.1992.262.1.E118>.
53. Pollizzi, K.N., and Powell, J.D. (2014). Integrating canonical and metabolic signalling programmes in the regulation of T cell responses. *Nat. Rev. Immunol.* 14, 435–446. <https://doi.org/10.1038/nri3701>.
54. Colombani, J., and Andersen, D.S. (2023). Drosophila TNF/TNFRs: At the crossroad between metabolism, immunity, and tissue homeostasis. *FEBS Lett.* 597, 2416–2432. <https://doi.org/10.1002/1873-3468.14716>.
55. Beckermann, K.E., Hongo, R., Ye, X., Young, K., Carbonell, K., Healey, D.C.C., Siska, P.J., Barone, S., Roe, C.E., Smith, C.C., et al. (2020). CD28 costimulation drives tumor-infiltrating T cell glycolysis to promote inflammation. *JCI Insight* 5, e138729. <https://doi.org/10.1172/jci.insight.138729>.
56. Frauwirth, K.A., Riley, J.L., Harris, M.H., Parry, R.V., Rathmell, J.C., Plas, D.R., Elstrom, R.L., June, C.H., and Thompson, C.B. (2002). The CD28 signaling pathway regulates glucose metabolism. *Immunity* 16, 769–777.
57. Jaeger-Ruckstuhl, C.A., Lo, Y., Fulton, E., Waltner, O.G., Shabaneh, T.B., Simon, S., Muthuraman, P.V., Correnti, C.E., Newsom, O.J., Engstrom, I.A., et al. (2024). Signaling via a CD27-TRAF2-SHP-1 axis during naive T cell activation promotes memory-associated gene regulatory networks. *Immunity* 57, 287–302. <https://doi.org/10.1016/j.immuni.2024.01.011>.
58. Bishop, E.L., Gudgeon, N., Fulton-Ward, T., Stavrou, V., Roberts, J., Boufersaoui, A., Tennant, D.A., Hewison, M., Raza, K., and Dimeloe, S. (2024). TNF-alpha signals through ITK-Akt-mTOR to drive CD4(+) T cell metabolic reprogramming, which is dysregulated in rheumatoid arthritis. *Sci. Signal.* 17, eadg5678. <https://doi.org/10.1126/scisignal.adg5678>.
59. Laplante, M., and Sabatini, D.M. (2012). mTOR signaling in growth control and disease. *Cell* 149, 274–293. <https://doi.org/10.1016/j.cell.2012.03.017>.
60. Triki, M., Rinaldi, G., Planque, M., Broekaert, D., Winkelkotte, A.M., Mavier, C.R., Janaki Raman, S., Vandekerke, A., Van Elsen, J., Orth, M.F., et al. (2020). mTOR Signaling and SREBP Activity Increase FADS2 Expression and Can Activate Sapienate Biosynthesis. *Cell Rep.* 31, 107806. <https://doi.org/10.1016/j.celrep.2020.107806>.
61. Hosios, A.M., Wilkinson, M.E., McNamara, M.C., Kalafut, K.C., Torrence, M.E., Asara, J.M., and Manning, B.D. (2022). mTORC1 regulates a lysosome-dependent adaptive shift in intracellular lipid species. *Nat. Metab.* 4, 1792–1811. <https://doi.org/10.1038/s42255-022-00706-6>.
62. Zeng, H., Yang, K., Cloer, C., Neale, G., Vogel, P., and Chi, H. (2013). mTORC1 couples immune signals and metabolic programming to establish T(reg)-cell function. *Nature* 499, 485–490. <https://doi.org/10.1038/nature12297>.

63. Su, W., Chapman, N.M., Wei, J., Zeng, H., Dhungana, Y., Shi, H., Saravia, J., Zhou, P., Long, L., Rankin, S., et al. (2020). Protein Prenylation Drives Discrete Signaling Programs for the Differentiation and Maintenance of Effector T<sub>reg</sub> Cells. *Cell Metab.* 32, 996–1011.e7. <https://doi.org/10.1016/j.cmet.2020.10.022>.
64. Pacella, I., Procaccini, C., Focaccetti, C., Miacci, S., Timperi, E., Faicchia, D., Severa, M., Rizzo, F., Coccia, E.M., Bonacina, F., et al. (2018). Fatty acid metabolism complements glycolysis in the selective regulatory T cell expansion during tumor growth. *Proc. Natl. Acad. Sci. USA* 115, E6546–E6555. <https://doi.org/10.1073/pnas.1720113115>.
65. Timilshina, M., You, Z., Lacher, S.M., Acharya, S., Jiang, L., Kang, Y., Kim, J.A., Chang, H.W., Kim, K.J., Park, B., et al. (2019). Activation of Mevalonate Pathway via LKB1 Is Essential for Stability of Treg Cells. *Cell Rep.* 27, 2948–2961.e7. <https://doi.org/10.1016/j.celrep.2019.05.020>.
66. Burzyn, D., Kuswanto, W., Kolodin, D., Shadrach, J.L., Cerletti, M., Jang, Y., Sefik, E., Tan, T.G., Wagers, A.J., Benoist, C., and Mathis, D. (2013). A special population of regulatory T cells potentiates muscle repair. *Cell* 155, 1282–1295. <https://doi.org/10.1016/j.cell.2013.10.054>.
67. Rabinowitz, J.D., and Enerbäck, S. (2020). Lactate: the ugly duckling of energy metabolism. *Nat. Metab.* 2, 566–571. <https://doi.org/10.1038/s42255-020-0243-4>.
68. Hui, S., Ghergurovich, J.M., Morscher, R.J., Jang, C., Teng, X., Lu, W., Esparza, L.A., Reya, T., Le, Z., Yanxiang Guo, J., et al. (2017). Glucose feeds the TCA cycle via circulating lactate. *Nature* 551, 115–118. <https://doi.org/10.1038/nature24057>.
69. Michalek, R.D., Gerriets, V.A., Jacobs, S.R., Macintyre, A.N., Maclver, N.J., Mason, E.F., Sullivan, S.A., Nichols, A.G., and Rathmell, J.C. (2011). Cutting edge: distinct glycolytic and lipid oxidative metabolic programs are essential for effector and regulatory CD4<sup>+</sup> T cell subsets. *J. Immunol.* 186, 3299–3303. <https://doi.org/10.4049/jimmunol.1003613>.
70. Howie, D., Cobbold, S.P., Adams, E., Ten Bokum, A., Necula, A.S., Zhang, W., Huang, H., Roberts, D.J., Thomas, B., Hester, S.S., et al. (2017). Foxp3 drives oxidative phosphorylation and protection from lipotoxicity. *JCI Insight* 2, e89160. <https://doi.org/10.1172/jci.insight.89160>.
71. Berod, L., Friedrich, C., Nandan, A., Freitag, J., Hagemann, S., Harmrolfs, K., Sandouk, A., Hesse, C., Castro, C.N., Bähre, H., et al. (2014). De novo fatty acid synthesis controls the fate between regulatory T and T helper 17 cells. *Nat. Med.* 20, 1327–1333. <https://doi.org/10.1038/nm.3704>.
72. Mensink, M., Schrama, E., Cuadrado, E., Amsen, D., de Kivit, S., and Borst, J. (2022). Proteomics reveals unique identities of human TGF-β-induced and thymus-derived CD4<sup>+</sup> regulatory T cells. *Sci. Rep.* 12, 20268. <https://doi.org/10.1038/s41598-022-23515-z>.
73. Wang, H., Franco, F., Tsui, Y.C., Xie, X., Trefny, M.P., Zappasodi, R., Mohmood, S.R., Fernández-García, J., Tsai, C.H., Schulze, I., et al. (2020). CD36-mediated metabolic adaptation supports regulatory T cell survival and function in tumors. *Nat. Immunol.* 21, 298–308. <https://doi.org/10.1038/s41590-019-0589-5>.
74. Pompura, S.L., Wagner, A., Kitz, A., LaPerche, J., Yosef, N., Dominguez-Villar, M., and Hafler, D.A. (2021). Oleic acid restores suppressive defects in tissue-resident FOXP3 Tregs from patients with multiple sclerosis. *J. Clin. Invest.* 131, e138519. <https://doi.org/10.1172/JCI138519>.
75. Xu, C., Fu, Y., Liu, S., Trittipi, J., Lu, X., Qi, R., Du, H., Yan, C., Zhang, C., Wan, J., et al. (2021). BATF Regulates T Regulatory Cell Functional Specification and Fitness of Triglyceride Metabolism in Restraining Allergic Responses. *J. Immunol.* 206, 2088–2100. <https://doi.org/10.4049/jimmunol.2001184>.
76. Morgan, P.K., Huynh, K., Pernes, G., Miotto, P.M., Mellett, N.A., Giles, C., Meikle, P.J., Murphy, A.J., and Lancaster, G.I. (2021). Macrophage polarization state affects lipid composition and the channeling of exogenous fatty acids into endogenous lipid pools. *J. Biol. Chem.* 297, 101341. <https://doi.org/10.1016/j.jbc.2021.101341>.
77. Rosas-Ballina, M., Guan, X.L., Schmidt, A., and Bumann, D. (2020). Classical Activation of Macrophages Leads to Lipid Droplet Formation Without *de novo* Fatty Acid Synthesis. *Front. Immunol.* 11, 131. <https://doi.org/10.3389/fimmu.2020.00131>.
78. Jarc, E., and Petan, T. (2020). A twist of FAtE: Lipid droplets and inflammatory lipid mediators. *Biochimie* 169, 69–87. <https://doi.org/10.1016/j.biochi.2019.11.016>.
79. Hsieh, W.Y., Zhou, Q.D., York, A.G., Williams, K.J., Scumpia, P.O., Kronenberger, E.B., Hoi, X.P., Su, B., Chi, X., Bui, V.L., et al. (2020). Toll-Like Receptors Induce Signal-Specific Reprogramming of the Macrophage Lipidome. *Cell Metab.* 32, 128–143.e5. <https://doi.org/10.1016/j.cmet.2020.05.003>.
80. Castoldi, A., Monteiro, L.B., van Teijlingen Bakker, N., Sanin, D.E., Rana, N., Corrado, M., Cameron, A.M., Hässler, F., Matsushita, M., Caputa, G., et al. (2020). Triacylglycerol synthesis enhances macrophage inflammatory function. *Nat. Commun.* 11, 4107. <https://doi.org/10.1038/s41467-020-17881-3>.
81. Alarcon-Barrera, J.C., von Hegedus, J.H., Brouwers, H., Steenvoorden, E., Ioan-Facsinay, A., Mayboroda, O.A., Ondo-Mendez, A., and Giera, M. (2020). Lipid metabolism of leukocytes in the unstimulated and activated states. *Anal. Bioanal. Chem.* 412, 2353–2363. <https://doi.org/10.1007/s00216-020-02460-8>.
82. Schlager, S., Goeritzer, M., Jandl, K., Frei, R., Vujic, N., Kolb, D., Strohmaier, H., Dorow, J., Eichmann, T.O., Rosenberger, A., et al. (2015). Adipose triglyceride lipase acts on neutrophil lipid droplets to regulate substrate availability for lipid mediator synthesis. *J. Leukoc. Biol.* 98, 837–850. <https://doi.org/10.1189/jlb.3A0515-206R>.
83. Dichlberger, A., Schlager, S., Lappalainen, J., Käkelä, R., Hattula, K., Butcher, S.J., Schneider, W.J., and Kovanen, P.T. (2011). Lipid body formation during maturation of human mast cells. *J. Lipid Res.* 52, 2198–2208. <https://doi.org/10.1194/jlr.M019737>.
84. Dichlberger, A., Schlager, S., Maaninka, K., Schneider, W.J., and Kovanen, P.T. (2014). Adipose triglyceride lipase regulates eicosanoid production in activated human mast cells. *J. Lipid Res.* 55, 2471–2478. <https://doi.org/10.1194/jlr.M048553>.
85. Marschallinger, J., Iram, T., Zardeneta, M., Lee, S.E., Lehallier, B., Haney, M.S., Pluvinage, J.V., Mathur, V., Hahn, O., Morgens, D.W., et al. (2020). Lipid-droplet-accumulating microglia represent a dysfunctional and proinflammatory state in the aging brain. *Nat. Neurosci.* 23, 194–208. <https://doi.org/10.1038/s41593-019-0566-1>.
86. Karagiannis, F., Masouleh, S.K., Wunderling, K., Surendar, J., Schmitt, V., Kazakov, A., Michla, M., Hölzel, M., Thiele, C., and Wilhelm, C. (2020). Lipid-Droplet Formation Drives Pathogenic Group 2 Innate Lymphoid Cells in Airway Inflammation. *Immunity* 52, 885. <https://doi.org/10.1016/j.immuni.2020.04.021>.
87. Shen, Y., Wen, Z., Li, Y., Matteson, E.L., Hong, J., Goronzy, J.J., and Weyand, C.M. (2017). Metabolic control of the scaffold protein TKS5 in tissue-invasive, proinflammatory T cells. *Nat. Immunol.* 18, 1025–1034. <https://doi.org/10.1038/ni.3808>.
88. Harayama, T., and Riezman, H. (2018). Understanding the diversity of membrane lipid composition. *Nat. Rev. Mol. Cell Biol.* 19, 281–296. <https://doi.org/10.1038/nrm.2017.138>.
89. Waddington, K.E., Robinson, G.A., Rubio-Cuesta, B., Chrifi-Alaoui, E., Andreone, S., Poon, K.S., Ivanova, I., Martin-Gutierrez, L., Owen, D.M., Jury, E.C., and Pineda-Torra, I. (2021). LXR directly regulates glycosphingolipid synthesis and affects human CD4<sup>+</sup> T cell function. *Proc. Natl. Acad. Sci. USA* 118, e2017394118. <https://doi.org/10.1073/pnas.2017394118>.
90. Qureshi, O.S., Zheng, Y., Nakamura, K., Attridge, K., Manzotti, C., Schmidt, E.M., Baker, J., Jeffery, L.E., Kaur, S., Briggs, Z., et al. (2011). Trans-endocytosis of CD80 and CD86: a molecular basis for the cell-extrinsic function of CTLA-4. *Science* 332, 600–603. <https://doi.org/10.1126/science.1202947>.
91. Stulnig, T.M., Berger, M., Sigmund, T., Raederstorff, D., Stockinger, H., and Waldhäusl, W. (1998). Polyunsaturated fatty acids inhibit T cell signal

- transduction by modification of detergent-insoluble membrane domains. *J. Cell Biol.* **143**, 637–644. <https://doi.org/10.1083/jcb.143.3.637>.
92. Obaseki, E., Adebayo, D., Bandyopadhyay, S., and Hariri, H. (2024). Lipid droplets and fatty acid-induced lipotoxicity: in a nutshell. *FEBS Lett.* **598**, 1207–1214. <https://doi.org/10.1002/1873-3468.14808>.
  93. Ma, E.H., Verway, M.J., Johnson, R.M., Roy, D.G., Steadman, M., Hayes, S., Williams, K.S., Sheldon, R.D., Samborska, B., Kosinski, P.A., et al. (2019). Metabolic Profiling Using Stable Isotope Tracing Reveals Distinct Patterns of Glucose Utilization by Physiologically Activated CD8(+) T Cells. *Immunity* **51**, 856–870.e5. <https://doi.org/10.1016/j.immuni.2019.09.003>.
  94. Ma, E.H., Dahabieh, M.S., DeCamp, L.M., Kaymak, I., Kitchen-Goosen, S.M., Oswald, B.M., Longo, J., Roy, D.G., Verway, M.J., Johnson, R.M., et al. (2024). <sup>13</sup>C metabolite tracing reveals glutamine and acetate as critical in vivo fuels for CD8 T cells. *Sci. Adv.* **10**, eadj1431. <https://doi.org/10.1126/sciadv.adj1431>.
  95. Perez-Riverol, Y., Bai, J., Bandla, C., García-Seisdedos, D., Hewapathirana, S., Kamatchinathan, S., Kundu, D.J., Prakash, A., Frericks-Zipper, A., Eisenacher, M., et al. (2022). The PRIDE database resources in 2022: a hub for mass spectrometry-based proteomics evidences. *Nucleic Acids Res.* **50**, D543–D552. <https://doi.org/10.1093/nar/gkab1038>.
  96. Smith, T.B., Patel, K., Munford, H., Peet, A., Tennant, D.A., Jeeves, M., and Ludwig, C. (2018). High-Speed Tracer Analysis of Metabolism (HS-TrAM). *Wellcome Open Res.* **3**, 5. <https://doi.org/10.12688/wellcomeopenres.13387.2>.
  97. Dawkins, E., Derks, R.J.E., Schifferer, M., Trambauer, J., Winkler, E., Simons, M., Paquet, D., Giera, M., Kamp, F., and Steiner, H. (2023). Membrane lipid remodeling modulates gamma-secretase processivity. *J. Biol. Chem.* **299**, 103027. <https://doi.org/10.1016/j.jbc.2023.103027>.
  98. Tsugawa, H., Cajka, T., Kind, T., Ma, Y., Higgins, B., Ikeda, K., Kanazawa, M., VanderGheynst, J., Fiehn, O., and Arita, M. (2015). MS-DIAL: data-independent MS/MS deconvolution for comprehensive metabolome analysis. *Nat. Methods* **12**, 523–526. <https://doi.org/10.1038/nmeth.3393>.
  99. Su, B., Bettcher, L.F., Hsieh, W.Y., Hornburg, D., Pearson, M.J., Blomberg, N., Giera, M., Snyder, M.P., Rafferty, D., Bensinger, S.J., and Williams, K.J. (2021). A DMS Shotgun Lipidomics Workflow Application to Facilitate High-Throughput, Comprehensive Lipidomics. *J. Am. Soc. Mass Spectrom.* **32**, 2655–2663. <https://doi.org/10.1021/jasms.1c00203>.
  100. Bingol, K., Li, D.W., Zhang, B., and Brüschweiler, R. (2016). Comprehensive Metabolite Identification Strategy Using Multiple Two-Dimensional NMR Spectra of a Complex Mixture Implemented in the COLMARm Web Server. *Anal. Chem.* **88**, 12411–12418. <https://doi.org/10.1021/acs.analchem.6b03724>.
  101. Dieterle, F., Ross, A., Schlotterbeck, G., and Senn, H. (2006). Probabilistic quotient normalization as robust method to account for dilution of complex biological mixtures. Application in 1H NMR metabonomics. *Anal. Chem.* **78**, 4281–4290. <https://doi.org/10.1021/ac051632c>.
  102. Kloos, D.P., Gay, E., Lingeman, H., Bracher, F., Müller, C., Mayboroda, O.A., Deelder, A.M., Niessen, W.M.A., and Giera, M. (2014). Comprehensive gas chromatography-electron ionisation mass spectrometric analysis of fatty acids and sterols using sequential one-pot silylation: quantification and isotopologue analysis. *Rapid Commun. Mass Spectrom.* **28**, 1507–1514. <https://doi.org/10.1002/rcm.6923>.
  103. Heinrich, P., Kohler, C., Ellmann, L., Kuerner, P., Spang, R., Oefner, P.J., and Dettmer, K. (2018). Correcting for natural isotope abundance and tracer impurity in MS-MS/MS- and high-resolution-multiple-tracer-data from stable isotope labeling experiments with IsoCorrector. *Sci. Rep.* **8**, 17910. <https://doi.org/10.1038/s41598-018-36293-4>.
  104. Kamphorst, J.J., Cross, J.R., Fan, J., de Stanchina, E., Mathew, R., White, E.P., Thompson, C.B., and Rabinowitz, J.D. (2013). Hypoxic and Ras-transformed cells support growth by scavenging unsaturated fatty acids from lysophospholipids. *Proc. Natl. Acad. Sci. USA* **110**, 8882–8887. <https://doi.org/10.1073/pnas.1307237110>.
  105. Jiang, W., Hua, R., Wei, M., Li, C., Qiu, Z., Yang, X., and Zhang, C. (2015). An optimized method for high-titer lentivirus preparations without ultracentrifugation. *Sci. Rep.* **5**, 13875. <https://doi.org/10.1038/srep13875>.
  106. Paulo, J.A., and Gygi, S.P. (2017). Nicotine-induced protein expression profiling reveals mutually altered proteins across four human cell lines. *Proteomics* **17**. <https://doi.org/10.1002/pmic.201600319>.

STAR★METHODS

KEY RESOURCES TABLE

REAGENT or RESOURCE	SOURCE	IDENTIFIER
<b>Antibodies</b>		
Mouse anti-CD3 (clone CLB-T3/4.E, 1XE, IgE isotype)	Sanquin	Cat# M1654
Mouse anti-CD28 (clone CLB-CD28/1, 15E8)	Sanquin	Cat# M1650
Mouse anti-TNFR2 (clone MR2-1)	Hycult Biotech	Cat# HM2007; RRID:AB_10987915
Mouse anti-CD4-PE-Cy7 (clone OKT4)	BioLegend	Cat# 317414; RRID:AB_571959
Mouse anti-CD127-BV421 (clone A019D5)	BioLegend	Cat# 351310; RRID:AB_10960140
Mouse anti-CD25-PE (clone 2A3)	BD Biosciences	Cat# 341011; RRID:AB_2783790
Mouse anti-CD45RA-FITC (clone HI100)	ImmunoTools	Cat# 21819453
Mouse anti-GPA33	Kindly provided by Prof. D. Amsen (Sanquin) <sup>39</sup>	N/A
Rat anti-FOXP3-APC (clone PCH101)	Invitrogen	Cat# 17-4776-42; RRID:AB_1603280
Armenian hamster anti-Helios-PE-Cy7 (clone 22F6)	BioLegend	Cat# 137236; RRID:AB_2565990
Mouse anti-CTLA-4-PE-Dazzle594 (clone L3D10)	BioLegend	Cat# 349922; RRID:AB_2566198
Rabbit anti-SLC16A3	Sigma-Aldrich	Cat# HPA021451; RRID:AB_1853663
Mouse anti-GAPDH	Cell Signaling Technology	Cat# 97166; RRID:AB_2756824
Rabbit anti-FASN	Cell Signaling Technology	Cat# 3180T; RRID:AB_2100796
Rabbit anti-SCD1	Cell Signaling Technology	Cat# 2794; RRID:AB_2183099
Anti-mouse IRDYE680	LI-COR Biosciences	Cat# 926-68020; RRID:AB_10706161
Anti-rabbit IRDYE800	LI-COR Biosciences	Cat# 926-32211; RRID:AB_621843
Anti-rabbit APC	Invitrogen	Cat# A-10931; RRID:AB_2534068
<b>Biological samples</b>		
Human buffy coat	Sanquin, Amsterdam, the Netherlands	N/A
<b>Chemicals, peptides, and recombinant proteins</b>		
IMDM Culture Medium	Gibco	Cat# 21980-032
FCS	Serana	Cat# S-FBS-SA-0150
Penicillin/streptomycin	Gibco	Cat# 15070-063
DMEM w/o glucose, L-glutamine, phenol red	Gibco	Cat# A14430-01
MEM Non-essential amino acid solution (100x)	Gibco	Cat# 11140-050
Dialyzed FCS	Life technologies	Cat# A33820
Recombinant human IL-2	DuPont Medical	N/A
LIVE/DEAD™ fixable near-IR dead cell stain kit, for 633 or 635 nm excitation	Invitrogen	Cat# L10119
Alexa Fluor 647 succinimidyl ester	Invitrogen	Cat# A37573
CellTrace Violet (CTV)	Invitrogen	Cat# C34557
CellTrace Yellow (CTY)	Invitrogen	Cat# C34567
4,4-Difluoro-5,7-Dimethyl-4-Bora-3a,4a-Diaza-s-Indacene-3-Dodecanoic Acid (BODIPY™ FL C12)	Invitrogen	Cat# D3922
6-(N-(7-Nitrobenz-2-oxa-1,3-diazol-4-yl)amino)-6-Deoxyglucose (6-NBDG)	Invitrogen	Cat# N23106
4',6-diamidino-2-phenylindole, dihydrochloride (DAPI)	Stemcell Technologies	Cat# 75004
HCS LipidTOX™ Deep Red neutral lipid stain	Invitrogen	Cat# H34477
Ficoll	Apotheek LUMC	Cat# 97902861

(Continued on next page)

**Continued**

REAGENT or RESOURCE	SOURCE	IDENTIFIER
Flow cytometry Stain buffer	BD Biosciences	Cat# 554656
Methyl <i>tert</i> -butyl ether (MTBE)	Honeywell Riedel-de Haen	Cat# 34875
Sodium pyruvate (100 mM)	Gibco	Cat# 1136-039
L-glutamine (200 mM)	Gibco	Cat# 25030-024
D-glucose	Merck	Cat# 108337
Sodium L-lactate	Sigma-Aldrich	Cat# 71718
tetrahydro-4-methylene-2R-octyl-5-oxo-3S-furancarboxylic acid (C75)	Cayman Chemical	Cat# 10005270
[U- <sup>13</sup> C <sub>6</sub> ]-glucose	Cambridge Isotopes	Cat# CLM-1396
[U- <sup>13</sup> C <sub>3</sub> ]-L-lactate	Sigma-Aldrich	Cat# 746258
Sodium sulfate	Fluka	Cat# 71961
N- <i>tert</i> -Butyldimethylsilyl-N-methyltrifluoroacetamide (MTBSTFA)	Sigma-Aldrich	Cat# 77626
N-methyl-N-trimethylsilyl-trifluoroacetamide (MSTFA) containing 1% Chlorotrimethylsilane	Thermo Scientific	Cat# TS-48915
N-trimethylsilyl-imidazole	Sigma-Aldrich	Cat# 394874
Opti-MEM	Gibco	11058-021
Polyethylenimine (PEI)	Polysciences	Cat# 23966-1
Puromycin dihydrochloride	Sigma-Aldrich	Cat# P7255
Radioimmunoprecipitation assay (RIPA) buffer	Thermo Scientific	Cat# 89900
Protease inhibitor cocktail	Roche	Cat# 11836153001
NuPAGE™ LDS sample buffer	Invitrogen	Cat# NP0007
NuPAGE™ 10% Bis-Tris gel	Invitrogen	Cat# NP0301BOX
NuPAGE™ MES SDS Running Buffer	Invitrogen	Cat# NP0002
Roche Western blocking reagent	Sigma-Aldrich	Cat# 11921673001
Western BLoT Immuno Booster	Takara	Cat# T7115A
BamHI-HF restriction enzyme	New England Biolabs	Cat# R3136S
NotI-HF restriction enzyme	New England Biolabs	Cat# R3189S
Sall-HF restriction enzyme	New England Biolabs	Cat# R3138S
XbaI restriction enzyme	New England Biolabs	Cat# R0145S
<b>Critical commercial assays</b>		
StraightFrom Buffy Coat CD4 MicroBead kit	Miltenyi Biotec	Cat# 130-114-980
FOXP3 transcription factor staining buffer set	Invitrogen	Cat# 00-5523-00
Intracellular fixation & permeabilization kit	Invitrogen	Cat# 88-8824-00
Pierce BCA Gold protein assay	Thermo Scientific	Cat# A53225
TMTpro™ 16plex label reagent set	Thermo Scientific	Cat# A44520
<b>Deposited data</b>		
RNA-seq data	GEO; De Kivit et al., <sup>30</sup> Mensink et al. <sup>43</sup>	Accession code GSE138604
Proteomics data	ProteomeXchange	Accession code PXD048504
<b>Experimental models: Cell lines</b>		
HEK293T cells	Netherlands Cancer Institute, Amsterdam, the Netherlands	RRID:CVCL_0063
Jurkat J16 cells	Netherlands Cancer Institute, Amsterdam, the Netherlands	RRID:CVCL_0065
<b>Recombinant DNA</b>		
pLKO.1-shControl construct: SHC002	Sigma-Aldrich	MISSION shRNA library
pLKO.1-shFASN construct: TRCN0000003128	Sigma-Aldrich	MISSION shRNA library

(Continued on next page)

**Continued**

REAGENT or RESOURCE	SOURCE	IDENTIFIER
pLKO.1-shSCD1 construct: TRCN000056613	Sigma-Aldrich	MISSION shRNA library
psPAX2 plasmid	Addgene	RRID:Addgene_12260
pMD2.G plasmid	Addgene	RRID:Addgene_12259
pCDH-EF1 plasmid	Addgene	RRID:Addgene_72266
hSLC16A3 VersaClone cDNA plasmid	R&D Systems	Cat# RDC0387
<b>Software and algorithms</b>		
FACSDiva software (version 8)	BD Biosciences	RRID:SCR_001456
FlowJo software (version 10.8.1)	BD Biosciences	RRID:SCR_008520
GraphPad Prism software (version 9.3.1)	GraphPad Software	RRID:SCR_002798
Qlucore Omics Explorer software (version 3.8)	Qlucore	<a href="https://qlucore.com">https://qlucore.com</a>
GSEA software (version 4.3.2)	UC San Diego and Broad Institute	RRID:SCR_003199
GEO2R (version R 4.2.2, Biobase 2.58.0, GEOquery 2.66.0, limma 3.54.0)	National Center for Biotechnology Information	RRID:SCR_016569
Ingenuity Pathway Analysis software (version 84978992)	QIAGEN	RRID:SCR_008653
Cytoscape software (version 3.9.1)	Cytoscape	RRID:SCR_003032
Cytoscape STRING app (version 2.0.1)	N/A	RRID:SCR_025009
Proteome Discoverer software (version 2.4)	Thermo Scientific	RRID:SCR_014477
Mascot (version 2.2.07)	Matrix Science	RRID:SCR_014322
MS-DIAL (version 4.70)	Riken	RRID:SCR_023076
TraceFinder software (version 5.1)	Thermo Scientific	RRID:SCR_023045
COLMARm web server database	Bingol et al. <sup>96</sup>	N/A
IsoCorrector R package	Bioconductor	<a href="https://doi.org/10.18129/B9.bioc.IsoCorrectorR">https://doi.org/10.18129/B9.bioc.IsoCorrectorR</a>
FAMetA R package	Alcoriza-Balaguer et al. <sup>51</sup>	N/A
Image Studio™ software (version 5.5.4)	LI-COR Biosciences	RRID:SCR_015795
<b>Other</b>		
BD FACSAria II cell sorter	BD Biosciences	RRID:SCR_018934
BD LSR II analyzer	BD Biosciences	RRID:SCR_002159
BD LSR Fortessa analyzer	BD Biosciences	RRID:SCR_018655
BD FACS Canto II	BD Biosciences	RRID:SCR_018056
Kinetex PS C18 column	Phenomenex	<a href="https://www.phenomenex.com/products/kinetex-hplc-column/kinetex-ps-c18">https://www.phenomenex.com/products/kinetex-hplc-column/kinetex-ps-c18</a>
Nexera series HPLC system	Shimadzu	<a href="https://www.ssi.shimadzu.com/products/liquid-chromatography/hplcuhplc/nexera-series/index.html">https://www.ssi.shimadzu.com/products/liquid-chromatography/hplcuhplc/nexera-series/index.html</a>
Sciex TripleTOF 6600 mass spectrometer	Sciex	<a href="https://www.sciex.com/landing-pages/tripletof6600plus">https://www.sciex.com/landing-pages/tripletof6600plus</a>
Sciex Lipidyzer	Sciex	<a href="https://sciex.com/">https://sciex.com/</a>
Sciex Qtrap 5500 mass spectrometer	Sciex	RRID:SCR_020517
Q-Exactive HF mass spectrometer	Thermo Scientific	RRID:SCR_020545
Vanquish autosampler and pump	Thermo Scientific	Cat# VH-P10-A-02, VH-A40-A-02, VH-C10-A-02
Sequant ZIC-pHILIC column	Merck	Cat# 150460
14 T Bruker Avance Neo NMR spectrometer	Bruker	<a href="https://www.bruker.com/en/products-and-solutions/mr/nmr/avance-neo-consoles.html">https://www.bruker.com/en/products-and-solutions/mr/nmr/avance-neo-consoles.html</a>
Agilent 8890 Gas Chromatography System	Agilent	RRID:SCR_019459
Agilent 5977B MS	Agilent	RRID:SCR_019420
VF-5ms column	Agilent	Cat# CP8944
CASY cell counter	OLS OMNI Life Science	<a href="https://www.ols-bio.de/products/cell-counter-casy">https://www.ols-bio.de/products/cell-counter-casy</a>

(Continued on next page)

**Continued**

REAGENT or RESOURCE	SOURCE	IDENTIFIER
Infinite® 200 PRO plate reader M Plex	Tecan	RRID:SCR_020543
Trans-Blot® Turbo™ system	Bio-Rad	RRID:SCR_023156
Nitrocellulose transfer packs	Bio-Rad	Cat# 1704158
Odyssey CLx infrared imager	LI-COR Biosciences	RRID:SCR_014579
UltiMate3000 HPLC system with Orbitrap Exploris480 mass spectrometer	Thermo Scientific	Cat# BRE725539
1cc C18 SPE cartridges	Oasis HLB, Waters	Cat# WAT094225

**EXPERIMENTAL MODEL AND STUDY PARTICIPANT DETAILS**

**Human material**

Human peripheral blood was obtained in accordance with the Declaration of Helsinki and the Dutch rules concerning the use of human materials from volunteer donors. Buffy coats from healthy, anonymized male or female donors aged 18 to 65 were collected after their written informed consent, as approved by the Ethical Advisory Council of Sanquin Blood Supply Foundation (License NVT0111.01), Amsterdam, the Netherlands. As human material was obtained from anonymized donors, no information regarding the gender, ancestry, race, ethnicity and socioeconomic status has been disclosed. The analyses were performed on tTregs and Tconvs in independent cultures that were obtained from the same buffy coat.

**METHOD DETAILS**

**T cell isolation and sorting**

CD4<sup>+</sup> T cells were directly isolated from buffy coats using the StraightFrom Buffy Coat CD4 MicroBead kit (Miltenyi Biotec). For cell sorting, these cells were stained with CD4-PE-Cy7, CD127-BV421 (BioLegend), CD25-PE (BD Biosciences), CD45RA-FITC (ImmunoTools) and GPA33-AF647<sup>30,39</sup> monoclonal antibodies (mAbs). The anti-GPA33 mAb was kindly provided by Prof. D. Amsen (Sanquin, Amsterdam, the Netherlands) and was conjugated in-house to Alexa Fluor 647 succinimidyl ester (Thermo Scientific) as previously described.<sup>39</sup> LIVE/DEAD near-IR dead cell stain (Invitrogen) was used to exclude dead cells. Naive tTregs and Tconvs were sorted based on CD4<sup>+</sup>CD25<sup>high</sup>CD127<sup>low</sup>CD45RA<sup>+</sup>GPA33<sup>high</sup> and CD4<sup>+</sup>CD25<sup>low</sup>CD127<sup>high</sup>CD45RA<sup>+</sup>GPA33<sup>int</sup> phenotypes, respectively, using a BD FACSAria II cell sorter with FACSDiva software (version 8) (BD Biosciences). Details regarding all antibodies, reagents, software and other materials used in this study are provided in the [key resources table](#).

**T cell expansion and restimulation**

After cell sorting (day 0), human naive tTregs and Tconvs were placed in 96-well round bottom plates (Corning, Thermo Fisher; 1 × 10<sup>4</sup> cells per well) and cultured in 100 μL IMDM (Capricorn Scientific) supplemented with 8% FCS (Serana) and penicillin/streptomycin (Gibco; 5000 U/mL) (T cell medium), at 37°C/5% CO<sub>2</sub>. To initiate T cell expansion, cells were cultured in the presence of IL-2 (DuPont Medical; 300 IU/mL) and soluble agonistic mAbs against CD3 (clone CLB-T3/4.E, IgE isotype, Sanquin, 0.1 μg/mL) and CD28 (clone CLB-CD28/1, Sanquin, 0.2 μg/mL). On day 4, 100 μL T cell medium supplemented with IL-2 (300 IU/mL) was added to the culture. From day 7 to day 11, cells were cultured in 24- or 6-well plates (Corning; 1 × 10<sup>6</sup> cells/mL) using fresh T cell medium supplemented with IL-2 (300 IU/mL), but without anti-CD3/28 mAbs. On day 11, T cells were collected and restimulated using anti-CD3 (0.1 μg/mL) combined with either anti-CD28 (0.2 μg/mL) or anti-TNFR2 (2.5 μg/mL) or left unstimulated for 24 h in the presence of IL-2 (300 IU/mL) ([Figure S1B](#)).

**Flow cytometry**

To assess the purity of expanded tTregs and Tconvs, T cells (5 × 10<sup>4</sup>) were washed in stain buffer (BD Biosciences) prior to fixation and permeabilization using the FXP3 transcription factor staining buffer set (Invitrogen) according to the manufacturer's instructions. Next, cells were stained using FXP3-APC (Invitrogen), Helios-PE-Cy7, CTLA-4-PE-Dazzle594 and TNFR2-PE (BioLegend) mAbs as indicated ([Figure S1C](#)). To assess SLC16A3 overexpression, Jurkat J16 cells were fixed using the intracellular fixation and permeabilization buffer set (Invitrogen) according to manufacturer's instruction. Cells were stained using rabbit anti-SLC16A3 pAbs (Sigma), followed by secondary anti-rabbit-APC pAbs (Invitrogen). LIVE/DEAD near-IR dead cell stain (Invitrogen) was used to exclude dead cells. Flow cytometric analysis was performed on a BD FACS Canto II, BD LSR II or BD Fortessa cell analyzer with FACSDiva software (version 8) (BD Biosciences). Data were analyzed using FlowJo software (version 10.8.1).

**Lipidomics**

tTregs and Tconvs were CD3/28- or CD3/TNFR2-stimulated or left unstimulated for 24 h in the presence of IL-2 (300 IU/mL) in a 6-well plate (Corning; 2 × 10<sup>6</sup> cells per mL). Cells were washed three times in PBS and cell pellets were snap-frozen and stored at -80°C until

further processing for untargeted or targeted lipidomics. Untargeted lipidomics was carried out as described elsewhere.<sup>97</sup> Briefly, lipids were extracted using methyl *tert*-butyl ether (MTBE; Honeywell Riedel-de Haën) from 2 to  $3 \times 10^6$  cells, depending on the number of cells available per biological replicate. After drying the organic extract under a gentle stream of nitrogen, lipids were dissolved in 200  $\mu$ L 50% 2-propanol and separated using reversed-phase chromatography (Kinetex C18 column, Phenomenex) employing a Nexera series HPLC system (Shimadzu) to deliver a gradient of water:acetonitrile 80:20 (eluent A) and water:acetonitrile:2-propanol 1:9:90 (eluent B). Both eluents contained 5 mM ammonium formate and 0.05% formic acid. Lipid detection was accomplished using a Sciex TripleTOF 6600 high resolution mass spectrometer (Sciex) and analysis took place in positive and negative electrospray ionization mode. The obtained mass spectra were analyzed using MS-DIAL v4.70.<sup>98</sup> Lipids were identified based on database matching of tandem mass spectra. All spectra were manually curated, and, for quality control purposes, lipid retention times were matched to side chain length and double bond numbers. For PCA, data were log-transformed and Pareto scaling was performed. To evaluate differences in lipids between Tconvs and tTregs, peak areas of detected lipid species were  $\log_{10}$  transformed, followed by hierarchical clustering of the lipid classes based on FA moieties. Lipids within each cluster were statistically analyzed as indicated.

Comprehensive targeted lipidomics was carried out using the Sciex Lipidyzer platform<sup>40,41</sup> operated with the shotgun lipidomics assistant software.<sup>99</sup> In short, lipids were extracted using MTBE from 5 to  $7 \times 10^6$  cells, depending on the number of cells available per biological replicate, after addition of deuterated internal standards. Targeted lipidomics was carried out using a flow-injection assay employing differential mobility spectrometry of lipid classes. Individual lipid species were quantified by monitoring characteristic mass transitions in multiple reaction monitoring mode on a Sciex Qtrap 5500 mass spectrometer. Detailed descriptions of the method and the quantification process have been described before.<sup>40,41</sup> For data analysis, the protein concentration per sample was determined using a Pierce BCA protein assay kit (Thermo Scientific). Data were normalized to protein content,  $\log_{10}$ -transformed and lipid species containing more than 25% missing values, which derived from signals below the detection limit of the system, were excluded from the analysis.

### Transcriptomics

Acquisition of bulk RNA-seq data from tTregs and Tconvs restimulated for 24 h via CD3, CD3/28 or CD3/TNFR2 was previously described<sup>30</sup> and data are publicly accessible in the GEO database under accession code GSE138604. Qlucore Omics Explorer software (version 3.8) was used to perform trimmed mean of M values (TMM) normalization. GRCh38.93.gtf was used as reference genome for alignment. Genes were excluded from downstream expression analysis when there were less than 20 mapped reads in at least 10 out of 18 samples. Genes with low overall variance due to the impact of noise were also excluded.

Principal component analysis (PCA) was used to visualize the data in two-dimensional space. Differential gene expression between two sample groups was determined by a Student's *t*-test with the Benjamini-Hochberg method for multiple testing correction and considered significant at  $FDR < 0.05$ . After Z score normalization, heat maps were created in GraphPad Prism (version 9.3.1).

Gene set enrichment analysis was performed with GSEA software (version 4.3.2) using gene sets from curated pathway databases Reactome and KEGG as listed in the Molecular Signatures Database (MSigDB) (available at <https://www.gsea-msigdb.org/gsea/index.jsp>). These gene sets were filtered for cell metabolism-related pathways as defined by Lim et al.<sup>42</sup> Raw microarray data from Lim et al.<sup>42</sup> were analyzed using the NCBI web application GEO2R with standard settings and subsequently compared to transcriptome data from the present study using GSEA. Mouse genes were converted to human orthologs before comparing  $\log_2$  fold changes.

Upstream transcriptional regulator analysis was performed using Ingenuity Pathway Analysis (version 84978992, QIAGEN). Target genes of upstream regulators were visualized in Cytoscape (version 3.9.1) using the STRING app (version 2.0.1). These gene sets were filtered for cell metabolism-related pathways as defined by Lim et al.<sup>42</sup>

### Glucose and FA uptake assay

For glucose and FA uptake assays, T cells ( $5 \times 10^4$ ) were washed in DMEM without glucose, sodium pyruvate, L-glutamine, FCS and phenol red (nutrient uptake medium, Gibco) and subsequently incubated with 6-NBDG (100  $\mu$ M, Invitrogen) or BODIPY-C12 (0.5  $\mu$ M, Invitrogen) in nutrient uptake medium for 45 min at 37°C/5% CO<sub>2</sub>. Cells were washed once in nutrient uptake medium containing 2% FCS prior to sample acquisition in stain buffer (BD Biosciences). DAPI (Stem Cell Technologies) was used to exclude dead cells. Flow cytometric analysis was performed on a BD FACS Canto II, BD LSR II or BD Fortessa cell analyzer with FACSDiva software (version 8) (BD Biosciences). Data were analyzed using FlowJo software (version 10.8.1).

### <sup>13</sup>C stable-isotope tracing

<sup>13</sup>C isotope tracer experiments and analysis of polar metabolites by LC-MS were performed as described in detail before.<sup>30</sup> For [U-<sup>13</sup>C<sub>6</sub>]-glucose tracing, media consisted of DMEM without glucose, pyruvate and L-glutamine, supplemented with penicillin/streptomycin, additional non-essential amino acids, 1 mM pyruvate, 2 mM L-glutamine (all from Gibco), 8% FCS (Serana) and 25 mM [U-<sup>13</sup>C<sub>6</sub>]-glucose (Cambridge Isotopes). For [U-<sup>13</sup>C<sub>3</sub>]-lactate tracing, media consisted of DMEM without glucose, pyruvate and L-glutamine, supplemented with penicillin/streptomycin, additional non-essential amino acids, 2 mM L-glutamine, 8% dialyzed FCS (all from Gibco), 1 mM glucose (Sigma), and 20 mM [U-<sup>13</sup>C<sub>3</sub>]-L-lactate (Sigma-Aldrich).

tTregs and Tconvs were restimulated in presence of IL-2 (300 IU/mL), with or without agonistic mAbs against CD3/28 or CD3/TNFR2 for 24 h. Cells were washed with ice-cold PBS and metabolites were extracted by adding 50  $\mu$ L ice-cold MS lysis buffer

(methanol/acetonitrile/ultrapure LC-MS grade water 2:2:1). Samples were shaken for 10 min, centrifuged for 15 min at 4°C and the supernatant was stored at -80°C until LC-MS analysis. LC-MS analysis was performed on a Q-Exactive HF mass spectrometer (Thermo Scientific) coupled to a Vanquish autosampler and pump (Thermo Scientific). Metabolites were separated using a Sequant ZIC-pHILIC column (2.1 × 150 mm, 5 μm, guard column 2.1 × 20 mm, 5 μm; Merck) using a linear gradient of acetonitrile and 20 mM (NH<sub>4</sub>)<sub>2</sub>CO<sub>3</sub>, 0.1% NH<sub>4</sub>OH in ULC/MS grade water (Biosolve) with a flow rate of 100 μL/min. The MS operated in polarity-switching mode with spray voltages of 4.5 kV and -3.5 kV. Metabolites were identified based on exact mass within 5 ppm and further validated in concordance with retention times of standards. Quantification was based on peak area using TraceFinder software (Thermo Scientific). Peak areas were normalized based on total signal and isotopomer distributions were corrected for natural abundance of <sup>13</sup>C based on unlabeled control samples.

Glucose-derived <sup>13</sup>C tracing in lipids was measured by NMR spectroscopy. Cell pellets were spun down at 750×g for 5 min at 4°C and cell pellets were washed with ice-cold PBS. Metabolites and lipids were extracted using a modified Bligh-Dyer extraction with methanol/chloroform/water, 2:2:1.8 (v/v/v). The bottom hydrophobic phase containing lipids was collected and dried under a gentle nitrogen gas flow. Extracts were then reconstituted in deuterated chloroform containing 0.03% (v/v) tetramethylsilane as NMR chemical shift reference. All samples were measured on a 14 T Bruker Avance Neo NMR spectrometer (600 MHz for <sup>1</sup>H) equipped with a 5 mm TCI cryoprobe (Bruker). Two NMR experiments were collected per sample: a 1D <sup>1</sup>H and a 2D <sup>1</sup>H-<sup>13</sup>C Heteronuclear Single Quantum Correlation (HSQC). For the latter, a modified pulse sequence<sup>96</sup> was used to enhance resolution in the <sup>13</sup>C dimension. Peak annotations were performed using the COLMARm web server database.<sup>100</sup> The splitting of peak of methyl protons from lipid moieties at (<sup>1</sup>H) 0.88 - (<sup>13</sup>C) 14.14 ppm was used to calculate the <sup>13</sup>C enrichment of the CH<sub>3</sub>-CH<sub>2</sub> group, which represents the pool FA chains. The splitting of peaks at (<sup>1</sup>H) 3.94 - (<sup>13</sup>C) 63.56 and (<sup>1</sup>H) 4.39 - (<sup>13</sup>C) 62.91 ppm were used to calculate the <sup>13</sup>C enrichment in the glycerol backbone of phospholipids while the peaks at (<sup>1</sup>H) 4.14 - (<sup>13</sup>C) 62.11 and (<sup>1</sup>H) 4.29 - (<sup>13</sup>C) 62.11 ppm were used to calculate the <sup>13</sup>C enrichment of glycerol backbone of TG. The integrals of these peaks were normalized based on the probabilistic quotients normalization method.<sup>101</sup> Quotients for each sample were determined from the integration of the total areas of the corresponding 1D <sup>1</sup>H spectra.

Mass isotopologue distribution (MID) of palmitate and cholesterol from cells cultured with the [U-<sup>13</sup>C<sub>3</sub>]-lactate tracing medium was measured by GC-MS on the lipid extracts of Tconvs and tTregs as previously reported with some modifications.<sup>102</sup> Cells were extracted as described above and the dried extracts were then reconstituted with 80 μL ethanol, 10 μL water and 10 μL aqueous NaOH solution (10 M) (Sigma-Aldrich). The mixtures were flushed with nitrogen gas and then saponified for 1 h at 70°C. Next, 35 μL of 6 M HCl (Sigma-Aldrich) were added, followed by extraction with MTBE and removal of water with sodium sulfate (Fluka). The extracts containing free FA and sterols were dried under a gentle stream of nitrogen. FA were derivatized by adding 25 μL *N-tert*-Butyldimethylsilyl-*N*-methyltrifluoroacetamide (MTBSTFA; Sigma-Aldrich) and incubating for 15 min at room temperature. Subsequently, sterols were derivatized with 25 μL of a mixture of *N*-methyl-*N*-trimethylsilyl-trifluoroacetamide (MSTFA) containing 1% Chlorotrimethylsilane (ThermoFisher) and 10% *N*-trimethylsilyl-imidazole (Sigma-Aldrich) and incubation for 15 min at 50°C. Finally, 50 μL *n*-hexane were added and all samples were analyzed using an Agilent 8890GC coupled to an Agilent 5977B MS equipped with an electron ionization source. The liner temperature was set at 280°C, transfer line at 280°C, source at 230°C and quadrupole at 150°C. 1 μL from each sample was injected and palmitate and cholesterol were separated on a VF-5ms column (Agilent; 30 m × 250 μm × 0.25 μm) with helium as carrier gas at a flowrate of 1.0 mL/min. The following temperature gradient was used: 1.5 min at 50°C, linear increase at 30 °C/min to 210°C, linear increase at 5 °C/min to 310°C, held for 4.0 min at 310°C.

The MID of palmitate and cholesterol were extracted from the intensities of the MS spectrum and corrected for natural <sup>13</sup>C abundance using the IsoCorrector R package.<sup>103</sup> The monoisotopic m/z of 313.3 was used for palmitate, and 368.3 for cholesterol. MIDs of cholesterol and palmitate were used for isotopomer spectral analysis (ISA)<sup>104</sup> using the R software package FAMetA<sup>51</sup> which modeled the parameters S (or *g(t)*) and I, which represent the rate of synthesis of a specific FA from <sup>13</sup>C-acetyl-CoA and the fraction of exogenous imported FA, respectively.

### Neutral lipid staining by flow cytometry

T cells (5 × 10<sup>4</sup>) were stimulated in T cell medium using anti-CD3 (0.1 μg/mL) combined with either anti-CD28 (0.2 μg/mL) or anti-TNFR2 (2.5 μg/mL) or left unstimulated for 24–96 h in the presence of IL-2 (300 IU/mL). Restimulated T cells were washed twice in stain buffer (BD Biosciences), followed by incubation with LIVE/DEAD near-IR dead cell stain for 10 min to discriminate between live and dead cells. Cells were fixed using the intracellular fixation & permeabilization kit (Invitrogen) and washed twice in stain buffer. Neutral lipids were stained using the HCS LipidTOX Deep Red neutral lipid stain (Invitrogen), for 1 h at RT. Cells were washed twice in stain buffer (BD Biosciences) prior to sample acquisition. Flow cytometric analysis was performed on a BD FACS Canto II, BD LSR II or BD Fortessa cell analyzer with FACSDiva software (version 8) (BD Biosciences). Data were analyzed using FlowJo software (version 10.8.1).

### T cell proliferation

To assess T cell proliferation, quiescent cells were washed once in PBS and labeled for 8 min with 5 μM CellTrace Violet or -Yellow (Invitrogen) at 37°C/5%CO<sub>2</sub>. Next, an equal volume of FCS was added for 5 min and cells were washed twice in IMDM supplemented with 8% FCS and penicillin/streptomycin. CellTrace-labeled T cells were restimulated and cultured in T cell medium as indicated for 96 h at 37°C/5% CO<sub>2</sub>. In some cultures, varying concentrations of D-glucose (Merck), sodium L-lactate (Sigma) or C75 (Cayman

Chemical) were added 1 h prior to and during restimulation cultures. After 96 h, cells were washed in stain buffer (BD Biosciences) and incubated with LIVE/DEAD near-IR dead cell stain for 10 min prior to sample acquisition. Flow cytometric analysis was performed on a BD FACS Canto II, BD LSR II or BD Fortessa cell analyzer with FACSDiva software (version 8) (BD Biosciences). Data were analyzed using FlowJo software (version 10.8.1). The division index was determined using the proliferation modeling tool within FlowJo software.

### T cell transductions

Knockdown of FASN and SCD1 in tTregs was conducted through lentiviral transduction of shRNA constructs derived from the MISSION shRNA library (Sigma-Aldrich) (shControl: SHC002; shFASN: TRCN0000003128; shSCD1: TRCN0000056613). Lentiviruses were made by transfecting  $7.5 \times 10^5$  HEK293T cells with a mixture of shRNA-targeting plasmids, psPAX2 and pMD2.G (1:1:1 M ratio, 15  $\mu$ g DNA) in OptiMEM (Invitrogen) containing 45  $\mu$ g polyethylenimine (PEI). Transfection medium was removed after 24 h and replaced by DMEM (Gibco) supplemented with 8% FCS and penicillin/streptomycin. After 24 h of culture, lentiviruses were harvested and used for transduction.

tTregs ( $1 \times 10^4$  cells/well) were stimulated for 48 h as described above prior to lentiviral transduction. Lentiviral supernatants were 0.45  $\mu$ m filtered and supplemented with IL-2 (300 IU/mL). T cells were spinoculated in 250  $\mu$ L viral supernatant per well at 850 $\times$ g for 90 min at 30°C and maintained for 96 h at 37°C/5%CO<sub>2</sub>. T cells were subsequently restimulated in 100  $\mu$ L T cell medium using soluble agonistic mAbs against CD3 (0.1  $\mu$ g/mL) and CD28 (0.2  $\mu$ g/mL) in the presence of IL-2 (300 IU/mL) and 0.5  $\mu$ g/mL puromycin (Sigma). After 48 h and 96 h of culture, 100  $\mu$ L T cell medium was added to the culture to maintain a final concentration of 300 IU/mL IL-2 and 1.0  $\mu$ g/mL puromycin. Prior to use in functional assays, cells were analyzed for viability using a CASY cell counter (OLS OMNI Life Science).

SLC16A3 was introduced in tTregs by lentiviral transduction of a cDNA encoding human SLC16A3. The SLC16A3 cDNA construct was generated by cloning an IRES-GFP fragment from the pMX-IRES-GFP vector (Addgene) into the pCDH-EF1 construct (a gift from Kazuhiro Oka, Addgene) using NotI and Sall restriction sites, obtaining the pCDH-EF1-IRES-GFP construct that served as empty vector control. Subsequently, the SLC16A3 cDNA was obtained from the human SLC16A3 VersaClone cDNA vector (R&D Systems) using the BamHI and XbaI restriction sites, followed by ligation into the pCDH-EF1-IRES-GFP construct. All restriction enzymes (NotI-HF, Sall-HF, BamHI-HF and XbaI) were obtained from New England Biolabs, and all vectors were sequence-verified.

Lentiviruses were made by transfecting  $5 \times 10^6$  HEK293T cells with a mixture of the pCDH1-EF1-SLC16A3-IRES-GFP or empty vector control, psPAX2 and pMD2.G (1:1:1 M ratio, 21  $\mu$ g DNA) in OptiMEM (Invitrogen) containing 63  $\mu$ g polyethylenimine (PEI). Transfection medium was removed after 24 h and replaced by Opti-MEM without phenol red (Gibco) supplemented with penicillin/streptomycin (Gibco). Lentiviruses were harvested 48 h and 96 h post-transfection, pooled and 0.45  $\mu$ m filtered, and concentrated by sucrose gradient centrifugation as previously described.<sup>105</sup>

For transductions, tTregs were flow cytometrically sorted and expanded as described above. On day 7, tTregs ( $5 \times 10^4$ ) were restimulated in 100  $\mu$ L T cell medium using soluble agonistic mAbs against CD3 (0.1  $\mu$ g/mL) and TNFR2 (2.5  $\mu$ g/mL) in the presence of IL-2 (300 IU/mL). After 24 h, 150  $\mu$ L concentrated viral supernatant was added per well and cells were centrifuged at 850 $\times$ g for 90 min at 30°C. Medium was replenished with complete T cell medium supplemented with IL-2 (300 IU/mL) the next day and maintained until day 14. On day 14, GFP<sup>+</sup> cells were flow cytometrically sorted on a BD FACSAria II cell sorter with FACSDiva software (version 8) (BD Biosciences), and used directly in a suppression assay.

### Western blot

FASN and SCD1 knockdown (KD) were validated in HEK293T cells (Netherlands Cancer Institute, Amsterdam). Cells ( $\geq 5 \times 10^5$  cells) were washed once in PBS and cell pellets were snap frozen in liquid N<sub>2</sub>. Lysates were prepared by resuspending the cell pellets in radioimmunoprecipitation assay (RIPA) buffer (Thermo Scientific), supplemented with a protease inhibitor cocktail (Roche). Protein concentrations were determined using BCA protein assay (Pierce) using an Infinite 200 PRO plate reader (Tecan). Gel electrophoresis was performed using 25  $\mu$ g of protein in NuPAGE LDS sample buffer (Invitrogen) on a 10% Bis-Tris NuPAGE gel (Invitrogen) in MES/SDS buffer (Invitrogen) for 1 h at 200 V. Proteins were transferred onto a nitrocellulose membrane with a Trans-Blot Turbo system (Bio-Rad) using nitrocellulose transfer packs (Bio-Rad) for 7 min at 1.3 A. Membranes washed three times in MilliQ water (Merck MilliPore) and subsequently stained with Ponceau S. Blocking of the membranes was done in Tris-buffered saline/0.1% Tween 20 (TBS-T) supplemented with 10% Roche Western blocking reagent (Sigma) for 1 h at RT, followed by primary antibody staining using mouse anti-GAPDH, rabbit anti-FASN, or rabbit anti-SCD1 (all from Cell Signaling Technology) overnight at 4°C in Immunobooster 1 solution (Takara). After six washing steps in TBS-T, membranes were simultaneously incubated with anti-mouse-IRDYE680 and anti-rabbit-IRDYE800 (both from LI-COR Biosciences) for 1 h at RT in Immunobooster 2 solution (Takara). Membranes were washed four times in TBS-T, once in PBS and once in MilliQ water prior to analysis on an Odyssey CLx infrared imager (LI-COR Biosciences). Fluorimetric analysis was performed using Image Studio software v5.5.4 (LI-COR Biosciences).

### Suppression assay

The suppressive function of tTregs was assessed as previously described.<sup>30</sup> In short, peripheral blood mononuclear cells (PBMC) obtained from healthy donor buffy coats by Ficoll density gradient centrifugation were labeled with CellTrace Violet or -Yellow as described above and co-cultured with tTregs in T cell medium in the presence of soluble agonistic mAbs against CD3 (0.05  $\mu$ g/mL)

for 96 h. Responder PBMC were allogeneic to the tTregs tested. After 96 h, cells were washed in stain buffer (BD Biosciences) and incubated with LIVE/DEAD near-IR dead cell stain for 10 min prior to sample acquisition on a BD FACS Canto II, BD LSR II or BD Fortessa cell analyzer with FACSDiva software (version 8) (BD Biosciences). The percentage of suppression was determined based on the percentage of proliferating (CellTrace<sup>+</sup>) cells within the live (IR-Dye<sup>-</sup>) and single cell gate, and was calculated using the formula:  $100 - ((\% \text{ proliferating responder cells in presence of tTregs} - \% \text{ background proliferation of responder cells}) / (\% \text{ proliferating responder cells in absence of tTregs} - \% \text{ background proliferation of responder cells})) \times 100\%$ .

### Proteomics

tTregs and Tconvs were restimulated in presence of IL-2 (300 IU/mL), with or without agonistic mAbs against CD3/28 or CD3/TNFR2 for 24 h. Tconvs and tTregs were separated into two TMTpro 16plex Label Reagent Sets (Thermo Scientific), with Jurkat J16 cells included in both sets as reference samples to allow for comparison. Cells were washed in ice-cold PBS and lysis, digestion and tandem mass tag (TMT) labeling were performed as described.<sup>106</sup> Lysis was performed using SDS lysis buffer (5% SDS, 100 mM Tris-HCl pH 7.6) and 5 U of benzonase nuclease (Thermo Scientific) by 4 min incubation at 95°C. Protein concentration was determined using Pierce BCA Gold protein assay (Thermo Scientific). 100 μg of protein of each sample was reduced with 5 mM TCEP. Reduced disulfide bonds were alkylated using 15 mM iodoacetamide. Excess iodoacetamide was quenched using 10 mM DTT. Protein lysates were precipitated using chloroform/methanol. Pellets were resolubilized in 40 mM HEPES pH 8.4 and digested using TPCK-treated trypsin (1:12.5 enzyme:protein ratio) overnight at 37°C. Peptide concentration was determined using Pierce BCA Gold protein assay. Tconvs and tTregs were restimulated in presence of IL-2 (300 IU/mL), with or without agonistic mAbs against CD3/28 or CD3/TNFR2 for 24 h. Tconvs and tTregs were separated into two TMTpro 16plex Label Reagent Sets (Thermo Scientific), with Jurkat J16 cells included in both sets as reference samples to allow for comparison. Cells were washed in ice-cold PBS and lysis, digestion and tandem mass tag (TMT) labeling were performed as described.<sup>106</sup> Lysis was performed using 5% SDS lysis buffer (100 mM Tris-HCl pH 7.6) and 5 U of benzonase nuclease (Thermo Scientific) by 4 min incubation at 95°C. Protein concentration was determined using Pierce BCA Gold protein assay (Thermo Scientific). 100 μg of protein of each sample was reduced with 5 mM TCEP. Reduced disulfide bonds were alkylated using 15 mM iodoacetamide. Excess iodoacetamide was quenched using 10 mM DTT. Protein lysates were precipitated using chloroform/methanol. Pellets were resolubilized in 40 mM HEPES pH 8.4 and digested using TPCK-treated trypsin (1:12.5 enzyme:protein ratio) overnight at 37°C. Peptide concentration was determined using Pierce BCA Gold protein assay.

Peptides were labeled with TMTpro Label Reagents (Thermo Scientific) in a 1:4 ratio by mass (peptides:TMT reagents), for 1 h at room temperature. Excess TMT reagent was quenched with 5 μL of 6% hydroxylamine for 15 min at room temperature. Samples were pooled and lyophilized. The TMT sample set was dissolved in 1 mL of 10 mM ammonium bicarbonate and fractionated using 1cc C18 SPE cartridges (Oasis HLB, Waters) with 15%, 17.5%, 20%, 25% and 35% acetonitrile buffers in 10 mM ammonium bicarbonate pH 8.4. TMT-labeled peptides were dissolved in water/formic acid (100/0.1 v/v) and subsequently analyzed twice by on-line C18 nanoHPLC MS/MS with a system containing an UltiMate3000 HPLC system and an Exploris480 mass spectrometer (Thermo Scientific). Fractions were injected onto a cartridge precolumn (300 μm × 5 mm, C18 PepMap, 5 μm, 100 Å) and eluted via a homemade analytical nano-HPLC column (50 cm × 75 μm, Reprosil-Pur C18-AQ 1.9 μm, 120 Å (Dr Maisch, Ammerbuch, Germany)). The gradient was run from 2% to 30% solvent B (20:80:0.1 water:acetonitrile:formic acid v/v) in 240 min. The nano-HPLC column was drawn to a tip of 10 μm and acted as electrospray needle of the MS source. The mass spectrometer was operated in data-dependent MS/MS mode with 3 s cycle time, with HCD collision energy at 36 V and recording of the MS2 spectrum in the orbitrap, with a quadrupole isolation width of 1.2 Da. In the master scan (MS1), resolution was 120,000, scan range 350–1200, and standard AGC target at maximum fill time of 50 ms. A lock mass correction on the background ion  $m/z = 445.12$  was used. Precursors were dynamically excluded after  $n = 1$  with an exclusion duration of 45 s, and with a precursor range of 20 ppm. Charge states 2–5 were included. For MS2 the first mass was set to 110 Da, and the MS2 scan resolution was 45,000 at an AGC target of 200% at maximum fill time of 60 ms.

Raw data were converted to peak lists using Proteome Discoverer software (version 2.4, Thermo Scientific), and submitted to UniProt (Homo sapiens, 20596 entries), using Mascot version 2.2.07 ([www.matrixscience.com](http://www.matrixscience.com)) for protein identification. Mascot searches were performed with 10 ppm and 0.02 Da deviation for precursor and fragment mass, respectively, and the enzyme trypsin was specified. Up to two missed cleavages were allowed. Methionine oxidation and acetyl on protein N terminus were set as fixed modifications. Protein and peptide FDR were set to 1%. Normalization was done on the total peptide amount. Identification of differentially expressed proteins with at least one unique peptide was performed using Proteome Discoverer. The CD28 costimulation samples from one donor were excluded from the analysis for technical reasons.

### QUANTIFICATION AND STATISTICAL ANALYSIS

Statistical analyses were performed using GraphPad Prism (version 10.2.3). Statistical analyses and data representation are described in the figure legends. In case data did not follow a normal distribution, a logarithmic transformation of the data was performed. A two-sided  $p < 0.05$  was considered statistically significant.

### ADDITIONAL RESOURCES

There are no additional resources related to the content of this study.